Journal of Thermal Analysis and Calorimetry (2019) 138:11–33
https://doi.org/10.1007/s10973-019-08090-2

Reversible formation of alcohol solvates and their potential use for heat storage

Kathrin Korhammer[1] · Judith Mihály[2] · Szabolcs Bálint[2,3] · László Trif[2] · Ádám Vass[2] · András Tompos[2] · Emília Tálas[2]

Received: 22 May 2018 / Accepted: 14 February 2019 / Published online: 5 March 2019

Abstract
In this study, $CaCl_2$- and $MgCl_2$–alcohol solvates of different stoichiometric quantities of ethyl alcohol (EtOH) and methyl alcohol (MeOH) were synthesized and characterized via coupled thermogravimetric–differential scanning calorimetry, thermogravimetric–mass spectrometric evolved gas analysis (TG-MS), spectroscopic analysis (Raman) methods as well as by X-ray diffraction. Correlations between the obtained calorimetric, thermodynamic, kinetic, and crystallographic data were carried out. The $CaCl_2$–alcohol systems seem suitable for heat storage based on the feasible recovery of the salt. However, Raman spectroscopic results revealed that the $MgCl_2$–EtOH solvates were instable compounds. Irreversible transformation of $MgCl_2$–alcohol solvates related to the formation of alkyl chloride appeared upon heating, as proven by TG-MS and Raman spectroscopic measurements. Pure salt–alcohol solvates could not be prepared under technically applicable conditions. The samples contained at least traces of water. Appearance of side reactions resulting in magnesium oxychlorides, oxyhydroxides, and possible release of HCl with cycling may contribute to corrosion of reactor components. Based on these considerations, $MgCl_2$–alcohol solvate systems are not recommended for heat storage.

Keywords Heat storage · $CaCl_2$ · $MgCl_2$ · Alcohol solvates · Alkyl chloride formation

Introduction

Storage and utilization of thermal energy are of utmost importance for a sustainable energy future. There are three main approaches in this field, e.g., sensible heat storage in water [1, 2], utilization of latent heat by phase change materials (PCM) [3–15], and conversion to chemical energy by different thermochemical reactions [16–22]. Heat storage via reversible thermochemical reactions has several benefits, such as high energy density per volume material and low long-term losses. Space can be a limiting factor for many practical applications. Most mobile applications, for instance, demand high energy densities in small volumes.

To date, the reaction of inorganic salts with water to form salt hydrates under heat release (1) has mainly been studied and optimized [23–26]. Alcohols are known to undergo similar reactions with salts (2). These reactions have only been studied in a casual manner in terms of their application in thermal energy storage [27, 28], although the high vapor pressure and low freezing point of EtOH and MeOH facilitate low-temperature applications unlike the aqueous adducts.

$$\mathrm{MX}\cdot(y-z)\mathrm{H_2O}\,(\mathrm{s})+z\mathrm{H_2O}\,(\mathrm{g})\rightleftharpoons\mathrm{MX}\cdot y\mathrm{H_2O}\,(\mathrm{s})+\Delta_{\mathrm{r}}H_1 \quad (1)$$

$$\mathrm{MX(s)}+z\mathrm{R\text{-}OH}\,(\mathrm{g})\rightleftharpoons\mathrm{MX}\cdot z\mathrm{R\text{-}OH}\,(\mathrm{s})+\Delta_{\mathrm{r}}H_2 \quad (2)$$

During the exothermic association reaction (discharging mode), the solid inorganic salt MX reacts with the gaseous alcohol R-OH forming the salt–alcohol solvate (alcoholate) MX·zR-OH, where z is the stoichiometric coefficient. The

✉ Emília Tálas
talas.emilia@ttk.mta.hu

[1] Leuphana University of Lüneburg, Universitätsallee. 1, 21335 Lüneburg, Germany

[2] Institute of Materials and Environmental Chemistry, Research Centre for Natural Sciences, Hungarian Academy of Sciences, Magyar tudósok körútja 2, 1117 Budapest, Hungary

[3] Semilab Semiconductor Physics Laboratory, Prielle Kornélia utca 2, 1117 Budapest, Hungary

chemical energy stored in the reaction is released as heat of reaction $\Delta_r H_2$. The reverse reaction (charging mode) is endothermic. Heat energy must be supplied to initiate the dissociation of the MX·zR-OH adduct. The gaseous product R-OH can be collected and condensed. Therefore, the storage volume can be reduced and the reaction products can be stored separately. As a result, a long-term storage without sensible heat losses is technically feasible. A schematic diagram of the operating principle of a closed thermochemical heat storage system is shown in Fig. 1.

Fast reaction kinetics, precise thermodynamic control, and low regeneration temperatures make salt–alcohol pairs an advantageous option. Recently, the suitability of EtOH solvates of $CaCl_2$, $MgCl_2$, and their mixtures as heat storage materials for practical implementations has been studied [29]. The EtOH sorption ability of $CaCl_2$ was better than that of $MgCl_2$. At high EtOH vapor pressures, over-stoichiometric EtOH uptake occurred. The $CaCl_2$–EtOH reaction system exhibited convenient sorption properties coupled with good multi-cyclic stability. Consequently, it has a great potential for low-grade thermal energy storage. However, poor reversibility appeared in case of the $MgCl_2$–EtOH system with increasing number of cycles, probably caused by irreversible decomposition that strongly reduced the material's sorption performance [29].

Due to the variety of synthesis procedures and conditions, an apparent discrepancy of the stoichiometry of salt alcoholates is found in the published literature. Moreover, present work on the energy storage density is limited. The aim of this work was to prepare and characterize salt–alcohol solvates of different stoichiometry based on anhydrous $CaCl_2$ and $MgCl_2$ by use of commercially available, specially non-purified chemicals with methods that can be relatively easily transposed into practice. The salt–alcohol solvates were prepared by direct synthesis from $CaCl_2$/$MgCl_2$ and EtOH/MeOH. This preparation method is based on the operating principle of a thermochemical heat store and can easily be adapted to practice. The focus was laid not only on the detailed comparative study of the calorimetric behavior, but also on the mapping of the heat-induced changes in these solvates. Besides coupled thermogravimetric–mass spectrometric (TG-MS) [30, 31], thermogravimetric analysis/differential scanning calorimetric (TGA/DSC) [32] techniques are generally applied in heat storage studies. We believed that Raman spectroscopy [33, 34] and X-ray powder diffraction (XRD) [35] methods are informative in sample characterization. Use of above techniques on structural changes in salt alcoholates is quite unique. We tried to find relationships between structural changes in the salt–alcohol solvates and the cyclic stability during repeated alcoholation/dealcoholation reactions observed earlier [29].

In solid state, the solvent molecules could be in a well-localized form and in solution they could be located in the first, second, and so on solvation shell. The interaction energies between the solvent molecules and solvated ions can vary over a broad range. Conducting single-crystal diffraction experiments for each composition was not

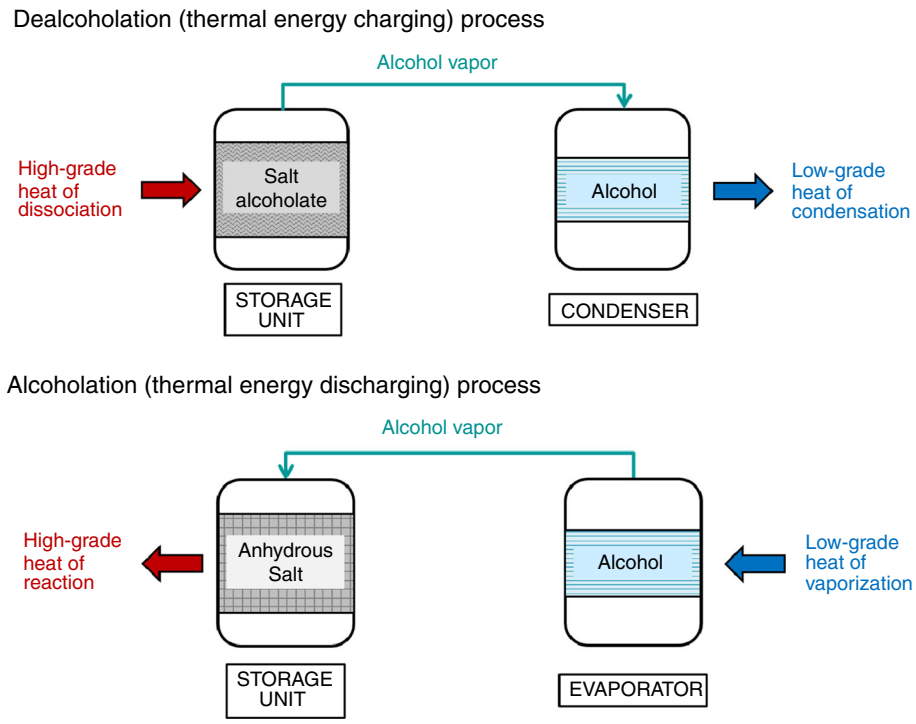

Fig. 1 Schematic diagram of the operating principle of a closed thermochemical heat storage system

possible and may be the subject of another work. Throughout this article, the term built-in form refers to the solvent molecules coordinated to the salt ions and also to the molecules loosely bound to the complexes studied, which dissociate upon crystallization or slightly elevating the temperature.

Experimental

Synthesis of salt–alcohol solvates

Anhydrous $CaCl_2$ powder (Merck, Ph Eur), anhydrous $MgCl_2$ powder (Roth, $\geq$ 98.5%), absolute MeOH (max. 0.003% H_2O, Merck), and absolute EtOH (max. 0.01% H_2O, Merck) were used as starting materials. The H_2O content of pure $CaCl_2$ and $MgCl_2$ samples as received was determined by TGA. The powdered salts contained only traces of H_2O.

Alcohol-salt pairs in four combinations, i.e., MeOH/$CaCl_2$, EtOH/$CaCl_2$, MeOH/$MgCl_2$, EtOH/$MgCl_2$, were prepared setting different alcohol/salt molar ratios (Table 1). The alcohol/salt stoichiometric ratios varied between 2 and 8 mol of EtOH or MeOH per mole anhydrous $CaCl_2$ or $MgCl_2$. Samples of 10 g of the respective salt were placed into a round bottom flask that was purged with dry nitrogen (N_2) prior to each alcoholate synthesis reaction. The flask was equipped with a magnetic stirrer and two thermometers. A stoichiometric amount of liquid alcohol was dropped onto the vigorously agitated salt under dry N_2 atmosphere, while both the temperature of the sample and the vapor phase were measured. Changes in textural and optical properties of the alcoholated salts were recorded. Preparation and denomination of the samples obtained are summarized in Table 1. The prepared samples were stored in closed glass vessels in a vacuum desiccator over P_2O_5.

Characterization methods

Simultaneous thermogravimetric analysis and differential scanning calorimetry

Experimental alcohol/salt ratios of the salt–alcohol solvates prepared at different theoretical stoichiometric molar ratios, according to Table 1, and associated heat absorptions were identified by simultaneous TGA/DSC. The horizontal furnace TGA/DSC 1 from Mettler Toledo was used. Specimens of 10–15 mg were uniformly placed into alumina crucibles of 70 µL volume and kept isothermally at 30 °C for 15 min to stabilize the sample. Dynamic runs were carried out by scanning the specimen from 30 to 180 °C with a temperature ramp of 3 °C min^{-1} at atmospheric pressure. During subsequent isothermal

Table 1 Preparation of salt–alcohol solvates by direct synthesis from liquid phase alcohols under neat conditions

Sample no.	Alcohol	Salt	Theoretical molar ratio/alcohol/salt	n_{acohol}/mol	n_{salt}/mol	$V_{alcohol}$/mL	m_{salt}/g
1	MeOH	$CaCl_2$	2:1	0.180	0.090	7.29	10
2	MeOH	$CaCl_2$	3:1	0.270	0.090	10.94	10
3	MeOH	$CaCl_2$	4:1	0.360	0.090	14.58	10
4	MeOH	$CaCl_2$	6:1	0.541	0.090	21.87	10
5	MeOH	$CaCl_2$	8:1	0.721	0.090	29.16	10
6	EtOH	$CaCl_2$	2:1	0.180	0.090	10.51	10
7	EtOH	$CaCl_2$	3:1	0.270	0.090	15.76	10
8	EtOH	$CaCl_2$	4:1	0.360	0.090	21.02	10
9	EtOH	$CaCl_2$	6:1	0.541	0.090	31.53	10
10	MeOH	$MgCl_2$	2:1	0.210	0.105	8.50	10
11	MeOH	$MgCl_2$	3:1	0.315	0.105	12.75	10
12	MeOH	$MgCl_2$	4:1	0.420	0.105	16.99	10
13	MeOH	$MgCl_2$	6:1	0.630	0.105	25.49	10
14	MeOH	$MgCl_2$	8:1	0.840	0.105	33.99	10
15	EtOH	$MgCl_2$	2:1	0.210	0.105	12.25	10
16	EtOH	$MgCl_2$	3:1	0.315	0.105	18.37	10
17	EtOH	$MgCl_2$	4:1	0.420	0.105	24.50	10
18	EtOH	$MgCl_2$	6:1	0.630	0.105	36.75	10

MeOH methanol, *EtOH* ethanol. Calculation of theoretical stoichiometric molar ratios at standard conditions (20 °C, 1 atm) using the respective molar masses and densities of the different substances

stabilization at the final temperature, the mass was recorded until the reaction went to completion. The TGA/DSC instrument was purged with N_2 at a flow rate of 50 mL min^{-1} during the entire measurement. Effects of buoyancy forces and temperature changes on the TGA and DSC signal were eliminated by automatic blank curve correction. For subtraction of the blank curve from the measurement curve, a blank curve was recorded under the same temperature conditions as the measurement curve, but using empty reference and sample crucibles. All measurements were performed under well-controlled laboratory conditions. The TGA/DSC device was calibrated with high purity metal standards (gallium, indium, lead, aluminum, and gold) over the temperature range of interest. For temperature and enthalpy calibration, the calibration substances were subjected to the same temperature and heating conditions as the samples analyzed. The measured onset temperature, which is assigned the start of the melting process, was compared with the reference melting point of the respective standard. The determined enthalpy of fusion was also validated by comparison with the reference value. The blank curve reproducibility was better than $\pm$ 10 μg over the whole temperature range. The standard deviation of the enthalpy reproducibility was given as $< 5\%$. Mass changes and heat powers were determined with a precision of $\pm$ 0.1 μg and $\pm$ 1 mW. The Mettler Toledo STARe software 11.00a was used for data processing.

Selected samples of the series of salt–alcohol solvates were characterized complimentary by Raman spectroscopy, TG-MS, and XRD. In case of the first two methods, N_2 atmosphere was used for sample handling.

Raman spectroscopy

Raman spectra of samples in closed glass ampoules held at room temperature were recorded with a dynamically aligned Bio-Rad (Digilab) dedicated FT-Raman spectrometer equipped with a Spectra Physics Nd–YAG laser (1064 nm) and high sensitivity liquid-N_2-cooled Ge detector. The excitation laser power used was about 250 mW at the samples. Increase in laser power up to 500 mW does not result in a significant change of the spectra that indicates the stability of the samples during the measurement. The resolution of the Raman instrument was ca. 4 cm^{-1}, and a backscattered geometry was used. For each spectrum, 256 individual spectra were averaged.

Thermogravimetric–mass spectrometric evolved gas analysis

The simultaneous thermogravimetric and mass spectrometric evolved gas analyses (TG-MS) were recorded on a Setaram LabsysEvo thermal analyzer, in high purity (99.9999%) helium atmosphere, with a flow rate of 80 mL min^{-1}. The measurements were done with a heating rate of 20 °C min^{-1}; the samples were weighed into 100 μL aluminum crucibles in inert (dry N_2) atmosphere. Exposure to moisture during sample transfer was prevented, and MS recording of evolved volatiles was enabled by closing the crucibles with aluminum lids pierced with a 700 micron hole by crimping. The measurements were performed in the 25–500 °C temperature range. The obtained results were baseline corrected and then evaluated with the thermal analyzer's processing software (AKTS Calisto Processing, ver. 1.41). Parallel with the thermogravimetric measurements, the analysis of the evolved gases/volatiles was carried out on a Pfeiffer Vacuum OmniStar™ gas analysis system coupled to the above-described TGA. The gas splitter and transfer line to the mass spectrometer were preheated to 250 °C. The scanned *m/z* interval was 5–79 amu, with a scan speed of 20 ms amu^{-1}. The mass spectrometer was operated in electron impact mode. During a measurement, the total ion current (TIC), the discrete ion current of all scanned masses (75 masses) and the analog spectra on each scan cycle (1 scan cycle was 1.5 s long) were obtained in parallel.

X-ray powder diffraction

XRD patterns were obtained in a Philips model PW 3710 based PW 1050 Bragg–Brentano parafocusing goniometer using CuK_α radiation ($\lambda = 0.15418$ nm), graphite monochromator and proportional counter. Samples were placed in an Anton-Paar HTK2000 high-temperature oven chamber. Prior to measurements, the chamber was flushed with high purity N_2 (99.9999%) and during XRD measurements a continuous slow N_2 flow was ensured. The temperature steps chosen for the "temperature programmed" XRD were based on the results of the TG-MS measurement of the appropriate sample. First, XRD patterns were recorded at room temperature, which was followed by stepwise in situ heating. The heating rate was 5 °C min^{-1}. XRD patterns were recorded at every temperature step. Finally, the samples were allowed to cool down (20 °C min^{-1}) and the room temperature XRD pattern was again measured. For the phase analysis, reference cards from the ICDD PDF-4 (2010) database were used.

Results and discussion

Preliminary results of the direct synthesis of salt–alcohol solvate

During the formation of the different salt alcoholate solvates, heat was evolved and resulted in a change in the temperature. The temperature change in the sample and the surrounding vapor phase was calculated from the difference between the respective initial and final temperatures. The initial sample temperatures ranged from 24 to 27 °C. The increase in temperature in both the sample and vapor chamber laid in the interval of 15–25 °C for almost all salt–alcohol pairs (Fig. 2). Rather fast reactions occurred and maximum temperatures of 40–56 °C were reached within a time of less than 3 min. In general, the temperature rise was higher in the solid phase than in the vapor phase, except for some outliers. For $CaCl_2$–alcohol solvates, higher temperature differences were measured when compared with that for $MgCl_2$–alcohol solvates. Since the temperature difference of both $CaCl_2$–MeOH and $CaCl_2$–EtOH solvates varied between 20 °C and 25 °C, irrespective of the alcohol/salt molar ratio, similar stoichiometric compositions of the different salt–alcohol solvates were considered. It is assumed that some heat dissipated into the ambient.

Lower temperature differences compared with that of $CaCl_2$ hydrates [36, 37] indicate lower heat outputs and corresponding enthalpies of reaction. Heterogeneous compounds were observed particularly for samples of higher stoichiometry. Some compositions consisted of two phases: a solid salt alcoholate phase and an excess liquid alcohol phase containing dissolved salt particles. Thus, further analysis was carried out using the solid salt–alcohol solvates only.

Results of TGA/DSC measurements of all samples

The composition of the different salt–alcohol solvates synthesized according to Table 1 was analyzed by TGA/DSC technique. The respective alcohol/salt molar ratios were derived from the change in sample mass recorded as a function of both time and temperature.

Thermal analysis of the $CaCl_2$–MeOH system

The total amount of MeOH uptake of $CaCl_2$ was calculated to be 4 (Table 2). Samples decomposed in 2–3 overlapping stages over a temperature domain of 33–145 °C (Fig. 3). The majority of MeOH was given off below 100 °C. Peak temperatures of 57–94 °C, 80–114 °C, and 95–118 °C were measured (Table 2). As depicted in Fig. 3, the mass loss rate of the first decomposition step, also referred to as rate of dealcoholation, increased with increasing stoichiometric ratio despite similar sample masses. At theoretical alcohol/salt ratios of 2 and 3, a compound doubly

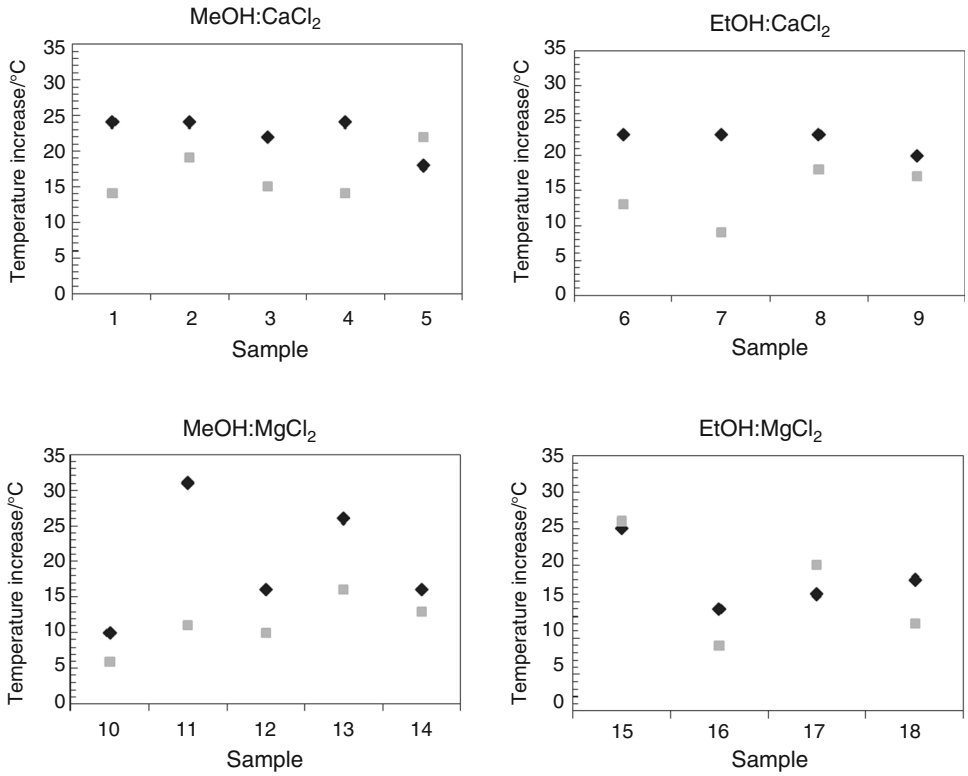

Fig. 2 Temperature increase during the synthesis of salt–alcohol solvates, according to Table 1. *MeOH* methanol; *EtOH* ethanol; diamond—sample, square—vapor chamber

Table 2 Data obtained from TGA/DSC measurements

Sample no.	Salt	Alcohol	z	X/ %	Step 1			Step 2			Step 3			Step 4						
					$T_{initial}$/ °C	T_{final}/ °C	T_{peak}/ °C	$T_{initial}$/ °C	T_{final}/ °C	T_{peak}/ °C	$T_{initial}$/ °C	T_{final}/ °C	T_{peak}/ °C	$T_{initial}$/ °C	T_{final}/ °C	T_{peak}/ °C	$\Delta_r H°$/ kJ mol^{-1}	$\Delta_r H°$/z/ kJ mol^{-1}	$\Delta_f H°$/ kJ mol^{-1}	E_m/ kJ kg^{-1}
1	$CaCl_2$	MeOH	2.1	38	54	100	92	100	113	110	113	127	118				101	49	1314	569
2	$CaCl_2$	MeOH	2.1	38	33	102	94	102	128	114							116	55	1337	649
3	$CaCl_2$	MeOH	3.1	47	34	100	93	100	117	108							108	35	1520	518
4	$CaCl_2$	MeOH	4.2	55	33	87	84	87	107	98	107	127	112				129	31	1771	525
5	$CaCl_2$	MeOH	4.0	54	33	63	57	63	85	80	85	145	95				151	38	1754	631
6	$CaCl_2$	EtOH	1.8	42	33	75	71	75	99	88	99	127	108	127	178	150	92	52	1303	475
7	$CaCl_2$	EtOH	1.9	44	35	78	71	78	101	92	101	127	118	127	178	168	122	64	1365	614
8	$CaCl_2$	EtOH	2.0	45	34	78	72	78	97	89	97	126	116	126	178	177	130	65	1394	642
9	$CaCl_2$	EtOH	1.8	42	34	72	68	72	100	87	100	132	121				99	55	132o	507
10	$MgCl_2$	MeOH	0.9	22	33	103	94	103	132	103	132	177	136				69	77	890	555
11	$MgCl_2$	MeOH	1.9	39	33	74	74	74	102	76	102	177	120				93	49	1115	594
12	$MgCl_2$	MeOH	2.1	42	33	71	65	71	105	78	105	177	122				105	50	1167	643
13	$MgCl_2$	MeOH	3.1	52	33	70	66	70	97	76	97	177	124				183	59	1447	943
14	$MgCl_2$	MeOH	4.1	58	33	76	67	76	108	102	108	136	122	136	177	158	175	43	1639	770
15	$MgCl_2$	EtOH	1.9	48	33	81	65	81	176	140							65	34	1153	354
16	$MgCl_2$	EtOH	2.3	53	33	74	62	74	143	130	143	177	153				90	39	1272	449
17	$MgCl_2$	EtOH	4.6	69	33	68	61	68	126	102	126	145	136	145	177	149	138	30	1860	448
18	$MgCl_2$	EtOH	3.5	63	33	76	67	76	142	101	142	177	149				158	45	1622	616

z, stoichiometric coefficient (ethanolation/methanolation level); X, mass loss; $T_{initial}$, initial temperature; T_{final}, final temperature; T_{Peak} peak temperature; $\Delta_r H°$, reaction enthalpy; $\Delta_r H°/z$, reaction enthalpy per mole EtOH/MeOH; $\Delta_f H°$, enthalpy of formation; E_m, gravimetric energy storage density. Step 1, step 2, step 3 and step 4 refer to the respective EtOH/MeOH release steps of the multi-stage dissociation reactions

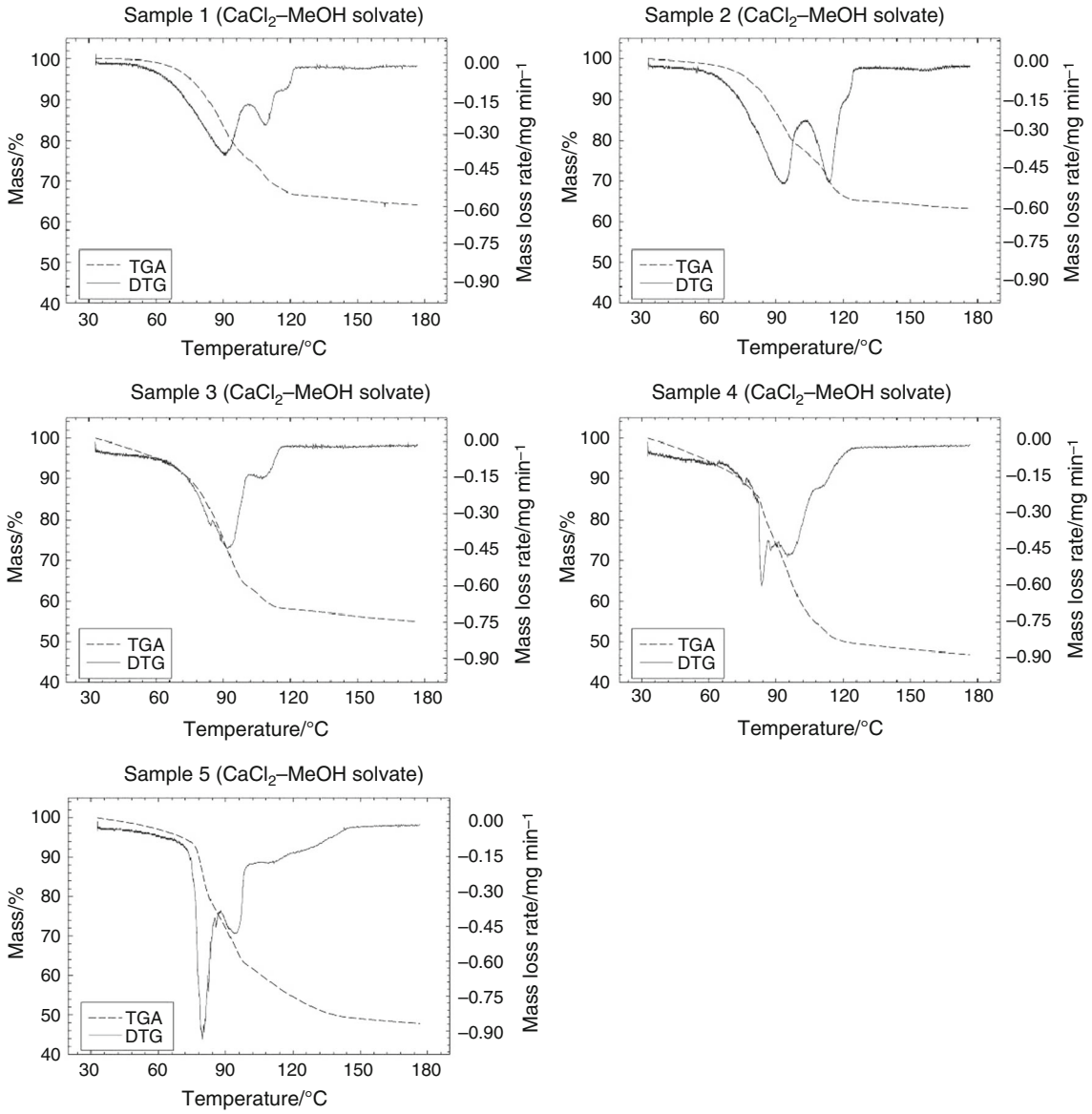

Fig. 3 Mass (TGA) and mass loss rate (DTG) curves of the dealcoholation of $CaCl_2$–MeOH solvates prepared in neat at different MeOH/$CaCl_2$ molar ratios (see Table 1), (measurement temperature interval: 30–180 °C; heating rate of 3 °C min^{-1}; 20 min isotherm at 180 °C)

coordinated with MeOH was the only $CaCl_2$–MeOH solvate found. This result is consistent with the findings of other authors [27, 38–42]. With excess of absolute MeOH, even a $CaCl_2$ trimethanolate and $CaCl_2$ tetramethanolate could be synthesized (Table 2). Note that samples prepared at higher theoretical alcohol/salt ratios were a heterogeneous mixture of two phases: a solid phase and a liquid phase. The latter was discarded from analysis. The formation of $CaCl_2$–MeOH complexes of different stoichiometry has been claimed by other researchers. Gmelin [43] has reported the existence of $CaCl_2$ monomethanolates and $CaCl_2$ trimethanolates that have been identified in a study conducted by Gerhold and Kahovec. Bonnell [44] and Menschutkin [45] have obtained $CaCl_2$ trimethanolates, too. MeOH solvates of $CaCl_2$ with a molar ratio of 4 [43–48] and 6 [49] have been characterized by different analysis methods. The standard reaction enthalpies were deduced from the DSC curve by peak integration and varied between 101 and 151 kJ mol^{-1} (Table 2).

Thermal analysis of the $CaCl_2$–EtOH system

In $CaCl_2$–EtOH solvate complexes (Fig. 4), the EtOH was evolved in up to four inseparable steps with peak temperature around 68–72 °C, 87–92 °C, 108–121 °C, and 150–177 °C, respectively (Table 2). The decomposition started roughly at 33 °C and was completed at around 178 °C. The major amount of EtOH was desorbed below

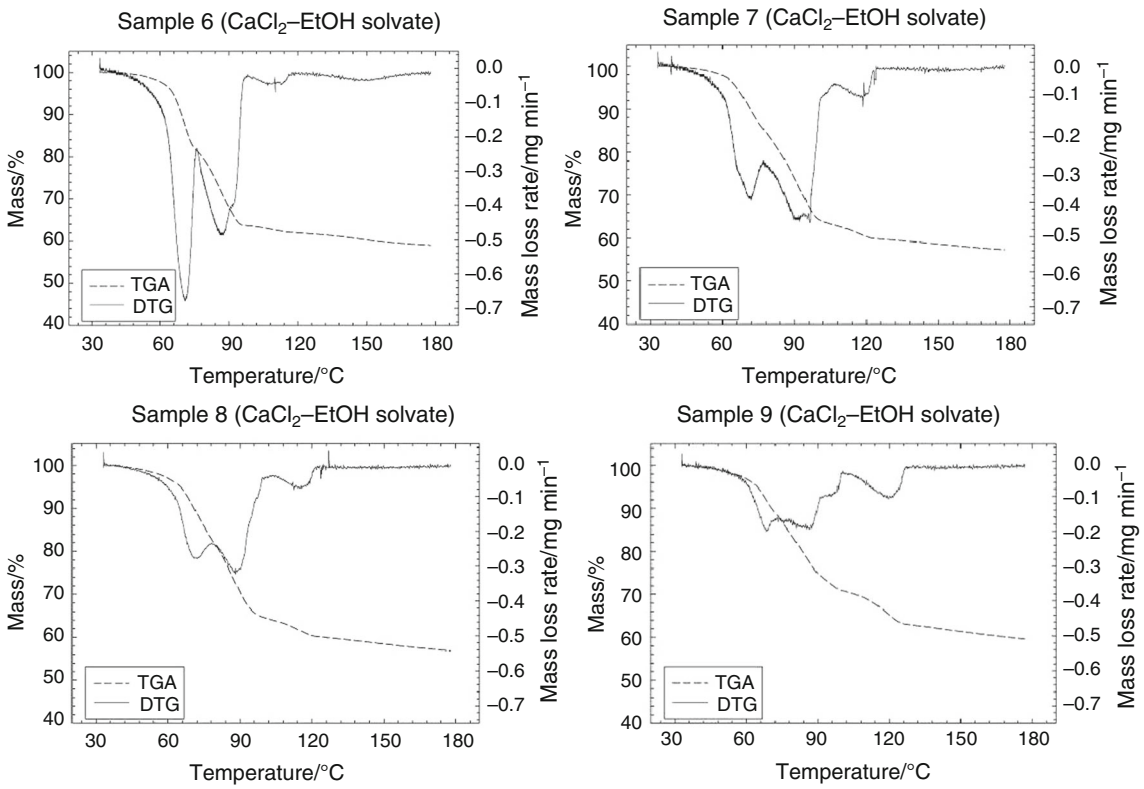

Fig. 4 Mass (TGA) and mass loss rate (DTG) curves of the dealcoholation of $CaCl_2$–EtOH solvates prepared in neat at different EtOH/$CaCl_2$ molar ratios (see Table 1), (measurement temperature interval: 30–180 °C; heating rate of 3 °C min^{-1}; 20 min isotherm at 180 °C)

100 °C. The rate of deethanolation varied over a broad range and was not reproducible, as shown in Fig. 4. The calculated percentage of mass loss (Table 2) clearly showed that in each sample only 2 mol of EtOH was adsorbed per mole of anhydrous $CaCl_2$. However, a variation in the standard enthalpy of reaction with values between 92 and 130 kJ mol^{-1} was observed. We suppose that $CaCl_2$ could only hold up to two molecules of EtOH under the experimental conditions studied, irrespective of the initial stoichiometric ratio we used during sample preparation. These data are consistent with the findings described in the literature [27, 50]. According to published literature data, EtOH forms also a number of other $CaCl_2$ ethanolates. Monoethanolates [43, 50, 51], triethanolates [43–45, 52, 53], and tetraethanolates [53–55] of $CaCl_2$ have been reported previously. Their existence was not proven in this study.

Thermal analysis of the $MgCl_2$–MeOH system

The experimental alcohol/salt ratios of the $MgCl_2$ methanolates prepared, as listed in Table 1, varied significantly from the theoretical ones. Methanolates of lower methanolation states were formed when the absolute MeOH was added in excess under the conditions studied. According to the obtained experimental data, about 1, 2, 3, and 4 MeOH molecules were sorbed by one molecule of $MgCl_2$ (Table 2). Samples 13 and 14 were deliquescent and therefore we presume that both physically and chemically attached MeOH was present. Depending on the amount of MeOH, the dissociation reaction proceeded in 3–4 incomplete steps (Fig. 5) over the temperature region of 33–177 °C with peak temperatures of 65–94 °C, 76–103 °C, 120–136 °C, and 158 °C, respectively (Table 2). Trace amounts of MeOH continued to evolve during isothermal stabilization at 180 °C until the demethanolation went to completion. As plotted in Fig. 5, the mass loss rates are in general lower compared with that of the $CaCl_2$–MeOH and $CaCl_2$–EtOH solvates. The DSC peak integration yielded standard reaction enthalpy values of 69–183 kJ mol^{-1} (Table 2). The obtained values were raised by increasing the alcohol/salt molar ratio. Recently, $MgCl_2$ monomethanolates have only been reported by Iyimen-Schwarz [51]. Furthermore, $MgCl_2$–MeOH species with stoichiometric numbers of coordinated MeOH molecules of 2 [42, 51, 56], 3 [51, 57], 4 [28, 42, 56, 58, 59], and 6 [47, 49, 56, 57, 60–66] have been identified in the literature.

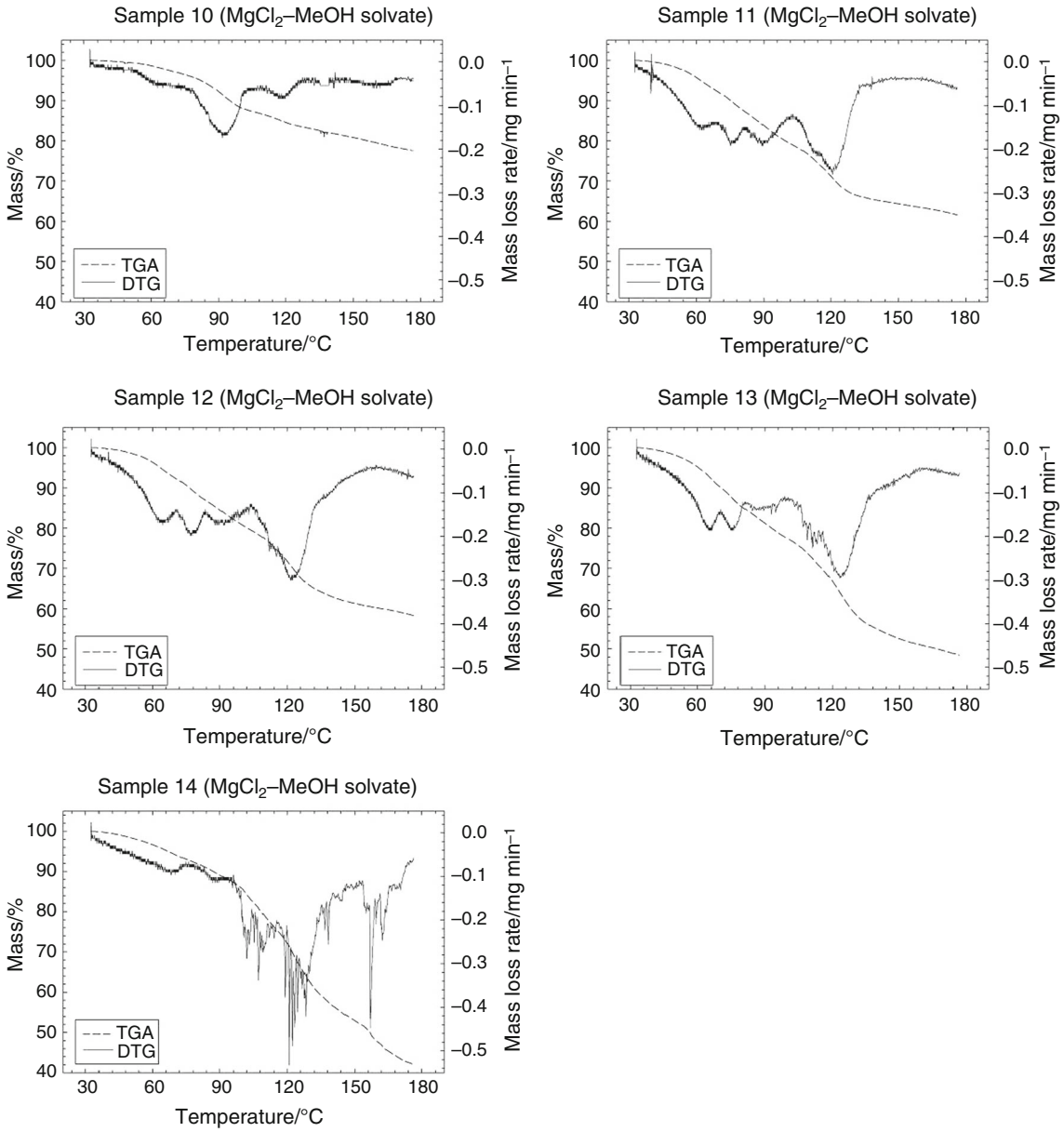

Fig. 5 Mass (TGA) and mass loss rate (DTG) curves of the dealcoholation of $MgCl_2$–MeOH solvates prepared in neat at different MeOH/$MgCl_2$ molar ratios (Table 1), (measurement temperature interval: 30–180 °C; heating rate of 3 °C min^{-1}; 20 min isotherm at 180 °C)

Thermal analysis of the $MgCl_2$–EtOH system

$MgCl_2$ formed ethanolates of different stoichiometry: stoichiometric ratios of 1.9, 2.3, 3.5, and 4.6 were identified under the experimental conditions studied (Table 2). The latter $MgCl_2$–4.6EtOH is doubtable as the maximum quantity of absolute EtOH added to anhydrous $MgCl_2$ was 4. The dissociation reaction occurred in 2–4 steps (Fig. 6) between 33 and 177 °C with peak temperatures at 61–67 °C, 101–140 °C, and 136–153 °C (Table 2). Trace amounts of EtOH were desorbed during the subsequent isothermal stabilization segment until the reaction went to completion, as observed for $MgCl_2$ methanolates (Fig. 5). The EtOH released in a stepwise manner was probably uncoordinated and coordinated EtOH. The samples 17 and 18 consisted of a two phase mixtures: liquid and solid phase. The latter was used for characterization studies. Mass loss rates between 0.2 and 0.4 mg min^{-1} were measured (Fig. 6). The calculated standard reaction enthalpies amounted to 65–158 kJ mol^{-1} (Table 2); the standard reaction enthalpies per mole EtOH were surprisingly low (30–45 kJ mol^{-1}), partly lower than the standard enthalpy of vaporization of EtOH (41.680 kJ mol^{-1}) [67]. $MgCl_2$–EtOH solvates have gained considerable interest among researchers for the synthesis of $MgCl_2$-supported Ziegler–Natta catalysts and subsequently a plethora of the

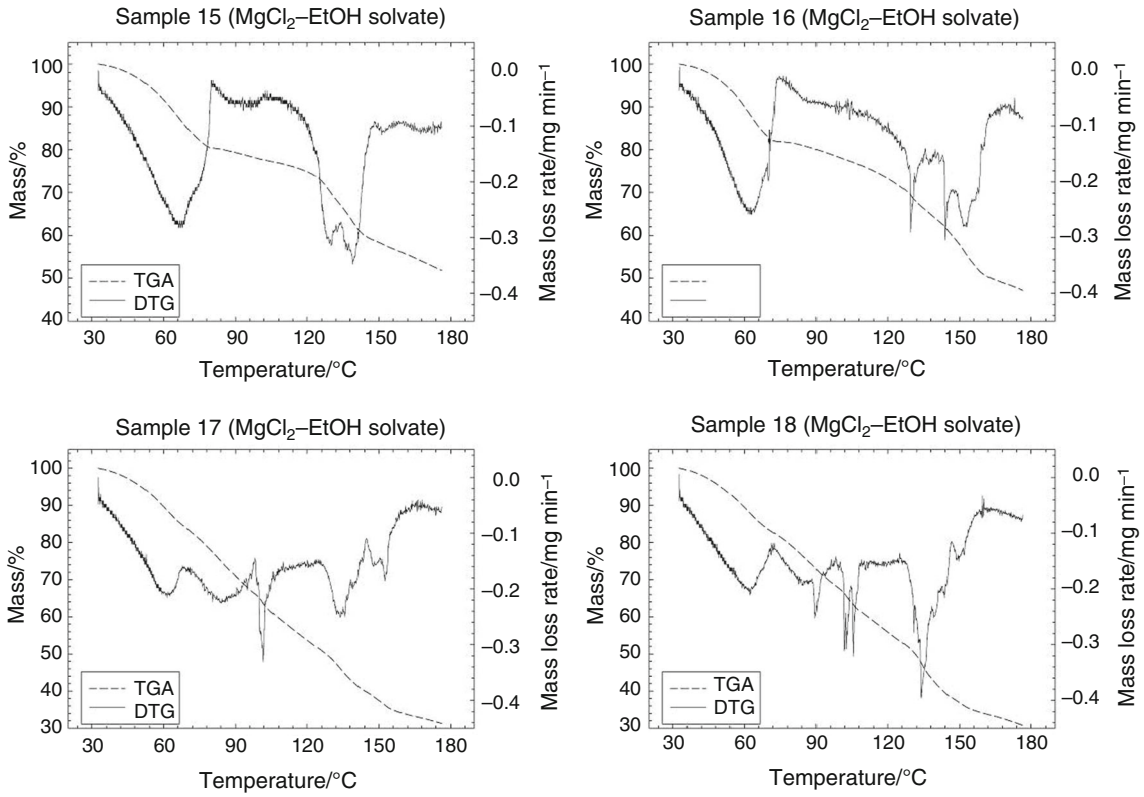

Fig. 6 Mass (TGA) and mass loss rate (DTG) curves of the dealcoholation of $MgCl_2$–EtOH solvates prepared in neat at different EtOH/$MgCl_2$ molar ratios (Table 1), (measurement temperature interval: 30–180 °C; heating rate of 3 °C min^{-1}; 20 min isotherm at 180 °C)

literature exists. Besides well-defined compounds, addition compounds of non-integer stoichiometry have also been identified in several studies. Iyimen-Schwarz [51], Tewell et al. [68], Chadwick and Severn [69], and Bart and Roovers [70] have prepared $MgCl_2$ ethanolates with a molar ratio of 0.47, 1, 1.1, and 1.25. The existence of $MgCl_2$ diethanolates has been proven by Multani [56] and Di Noto et al. [71]. Furthermore, EtOH solvates of $MgCl_2$ with molar ratios of 1.5 [72], 1.67 [68, 70], 2.05 and 2.1 [68, 69], 2.5 [70, 73], 2.8 [69, 72], and 3.33 [28, 70, 72] have been synthesized and investigated in detail. Complex compounds with higher stoichiometry of 4, 4.5, and 5 have been obtained by Bart and Roovers [70], Multani [56], and Tewell et al. [68]. The maximum coordination number observed in $MgCl_2$–EtOH complexes has been 6 according to various authors [56, 57, 63, 65–67, 70–72, 74, 75].

Comparing the decompositions temperatures of $CaCl_2$ alcohol solvates indicates that obviously MeOH was stronger associated with the metal chloride than EtOH. For instance, the EtOH evolution from $CaCl_2$–EtOH solvates started at lower temperatures than the desorption of MeOH from $CaCl_2$–MeOH solvates; the last MeOH molecule was liberated at higher temperatures than the last EtOH molecule. This means that during thermal cycling, EtOH can be liberated with lower energy than MeOH. Analogous reaction behavior was observed for $MgCl_2$ alcohol solvates. Moreover, $MgCl_2$–alcohol solvates showed lower dealcoholation rates and thus slower alcoholation/dealcoholation reactions are assumed in comparison with $CaCl_2$ alcohol solvates.

Energy analysis

Variation in the coordination numbers of the salt–alcohol solvates cited in the references and this study could be the result of the diversity in the synthesis procedures and conditions. According to Bart and Roovers [70], the synthesis method plays a crucial role with regard to the nature of the reactants. Salt–alcohol solvates can be prepared by direct synthesis, solution crystallization and elimination of excess solvent, or recrystallization, for example. The alcohol coordinates to the alkaline earth metal cations to form complexes with variable stoichiometry and structural properties that exist either in the solid state or in solution.

Note that the calculated enthalpies of reaction and dissociation (Table 2) tend to be inaccurate as no quantitative differentiation between alcohol molecules and possible H_2O molecules coordinated to one molecule of salt could be made at this stage. Samples contained probably trace amounts of H_2O that were neglected, since the freshly

prepared samples were immediately characterized via TGA/DSC.

A linear regression analysis of the experimentally obtained standard enthalpies of dissociation as a function of the number of alcohol molecules revealed that the applied model fitted well the data (Fig. 7). The coefficient of determination was close to one for each reaction system. Evidently, the standard enthalpy of dissociation increased along the homologous series of the alcohols studied. EtOH solvates possessed higher enthalpies of formation compared to MeOH solvates. The Ca^{2+} ion is of higher charge than the Mg^{2+} ion and has a greater polarizing power. Therefore, the standard enthalpies of formation of $CaCl_2$–alcohol complexes are comparatively higher.

The best fit (R^2 = 0.9981) was achieved with the $CaCl_2$–EtOH reaction system confirming its chemical stability. The calculated enthalpies of dissociation for all $CaCl_2$–2EtOH solvates analyzed were in the range of 1303–1394 kJ mol^{-1} (Table 2) and coincided with formation enthalpy and dissociation enthalpy data given in the published literature [27, 50] (Table 3). $CaCl_2$–EtOH complexes of higher ethanolated states as reported by Parker et al. [53] and those of lower ethanolated states [50, 51] could not be synthesized under the experimental conditions applied.

The $CaCl_2$–MeOH system exhibited an acceptable fit with a coefficient of determination of R^2 = 0.9967. The enthalpies of dissociation of the $CaCl_2$–2MeOH solvates with values of 1314 kJ mol^{-1} and 1337 kJ mol^{-1}, respectively, (Table 2) were slightly higher than literature values [27, 38, 42, 51] (Table 3). Enthalpies of reaction and formation/dissociation for $CaCl_2$–3MeOH and $CaCl_2$–4MeOH have not been determined yet. The enthalpy of dissociation of $CaCl_2$–3MeOH and of $CaCl_2$–4MeOH was estimated at 1520 kJ mol^{-1} and 1771 kJ mol^{-1}/1754 kJ mol^{-1}, respectively. The enthalpy of dissociation of $CaCl_2$–MeOH complexes increased with the number of alcohol molecules indicating a linear relationship. However, a nonlinear relationship could be observed when the standard enthalpies of reaction per mole of alcohol $\frac{\Delta_r H^0}{z}$ were compared (Table 2). At levels of methanolation higher than 2, the enthalpies of reaction per mole MeOH varied between 31 and 38 kJ mol^{-1} (Table 2), which are close to the standard enthalpy of vaporization of MeOH (37.965 kJ mol^{-1}) [67]. Apparently, up to 2 molecules could be chemically bound as a ligand. In MeOH solvates of $CaCl_2$ with higher molar ratios, the inclusion of MeOH molecules or physical incorporation of molecules into the crystal lattice could have caused the decrease in the standard enthalpy of reaction per mole of MeOH.

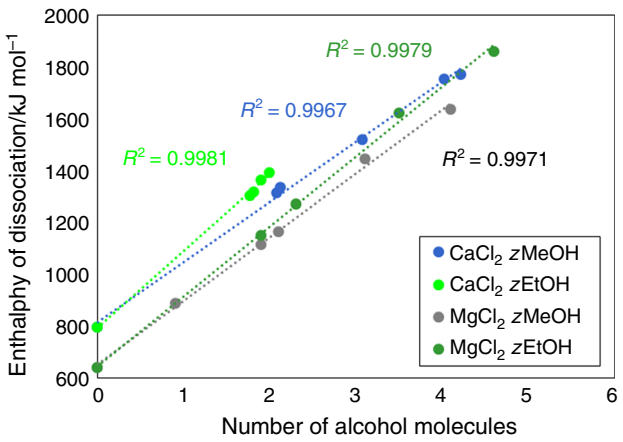

Fig. 7 Experimentally obtained standard enthalpies of dissociation of various salt–alcohol solvates plotted against the number of alcohol molecules evolved during the dissociation reaction, *MeOH* methanol, *EtOH* ethanol. Linear regression analysis was applied to determine the coefficient of determination (R-squared)

A linear relation between the enthalpy of dissociation and the number of alcohol molecules was also found for $MgCl_2$–EtOH and $MgCl_2$–MeOH solvate complexes (Fig. 7). The R-squared values of the $MgCl_2$–EtOH and $MgCl_2$–MeOH systems were R^2 = 0.9979 and R^2 = 0.9971, respectively. Reference data are rarely available. Iyimen-Schwarz [51] has collected the enthalpies of formation and dissociation of $MgCl_2$–1EtOH, $MgCl_2$–1MeOH, and $MgCl_2$–3MeOH solvates from thermal cycling tests by DSC technique (Table 4). When compared with values determined in this study, a significant deviation appeared. The values given by Iyimen-Schwarz [51] are mean values averaged over 13 cycles for $MgCl_2$–MeOH solvates and 10 cycles for $MgCl_2$–EtOH solvates. Maximum formation and dissociation enthalpy values of 31 kJ mol^{-1}/− 34 kJ mol^{-1} and 111 kJ mol^{-1}/−− 103 kJ mol^{-1} were derived for $MgCl_2$–1MeOH and $MgCl_2$–3MeOH. In the present study, the enthalpies of dissociation of $MgCl_2$–1MeOH, $MgCl_2$–2MeOH, $MgCl_2$–3MeOH, and $MgCl_2$–4MeOH ranged from 891 to 1639 kJ mol^{-1} (Table 2). The calculated enthalpies of reaction per mole MeOH of 43–77 kJ mol^{-1} (Table 2) were higher than the standard enthalpy of vaporization of MeOH. However, the enthalpies of reaction per mole EtOH with values of 30–45 kJ mol^{-1} (Table 2) were lower in comparison with the enthalpy of vaporization of EtOH (42 kJ mol^{-1}) [67]. Iyimen-Schwarz [51] has obtained even lower enthalpies of formation and dissociation and, respectively, enthalpies of reaction per mole of EtOH for $MgCl_2$–EtOH solvates (Table 3). These inconsistent and unreliable experimental results are ascribed to inherent instability issues of the $MgCl_2$–alcohol solvates.

To assess the suitability of the various salt–alcohol solvate systems for low-temperature heat storage, the gravimetric energy density was calculated from the

Table 3 Data available in the literature on experimental and theoretical standard enthalpies of reaction per mole salt alcoholate $\Delta_r H°$ and standard enthalpies of formation/dissociation $\Delta_f H°$ of $CaCl_2$–MeOH and $CaCl_2$–EtOH complexes of different stoichiometry z

	$z = 1$		$z = 2$		$z = 3$		$z = 4$	
	$\Delta_r H°$/ kJ mol^{-1}	$\Delta_f H°$/ kJ mol^{-1}	$\Delta_r H°$/ kJ mol^{-1}	$\Delta_f H°$/ kJ mol^{-1}	$\Delta_r H°$/ kJ mol^{-1}	$\Delta_f H°$/ kJ mol^{-1}	$\Delta_r H°$/ kJ mol^{-1}	$\Delta_f H°$/ kJ mol^{-1}
$CaCl_2$–MeOH complexes								
Aristov et al. [38]			− 120	− 1317				
Carling et al. [27]			− 113	− 1310				
Iyimen-Schwarz [51]			− 102	− 1299				
Iyimen-Schwarz [51]			103	1300				
Offenhartz et al. [42]			− 103	− 1300				
$CaCl_2$–EtOH complexes								
Carling et al. [27]			− 127	− 1393				
Iyimen-Schwarz [51]	− 17	− 1048						
Iyimen-Schwarz [51]	26	1057						
Mar and Carling [50]	51	1082	− 103	− 1369				
Mar and Carling [50]	− 51	− 1082	105	1371				
Parker et al. [53]					− 172	− 1673	− 219	− 1956

For the calculation of missing enthalpy data, a standard enthalpy of formation of − 796 kJ mol^{-1} for solid $CaCl_2$, of − 201 kJ mol^{-1} for gaseous MeOH and of − 235 kJ mol^{-1} for gaseous EtOH was used, respectively [82]

Table 4 Data available in the literature on experimental and theoretical standard enthalpies of reaction per mole salt alcoholate $\Delta_r H°$ and standard enthalpies of formation/dissociation $\Delta_f H°$ of $MgCl_2$–MeOH and $MgCl_2$–EtOH complexes of different stoichiometry z

	z = 1		z = 2		z = 3		z = 4	
	$\Delta_r H°$ /kJ mol^{-1}	$\Delta_f H°$ /kJ mol^{-1}	$\Delta_r H°$ /kJ mol^{-1}	$\Delta_f H°$ /kJ mol^{-1}	$\Delta_r H°$ /kJ mol^{-1}	$\Delta_f H°$ /kJ mol^{-1}	$\Delta_r H°$ /kJ mol^{-1}	$\Delta_f H°$ /kJ mol^{-1}
$MgCl_2$–MeOH complexes								
Iyimen-Schwarz [51]	− 19	− 861			− 52	− 1295		
Iyimen-Schwarz [51]	21	863			67	1310		
$MgCl_2$–EtOH complexes								
Iyimen-Schwarz [51]	− 17	− 893						
Iyimen-Schwarz [51]	19	895						

For the calculation of missing enthalpy data, a standard enthalpy of formation of − 641 kJ mol^{-1} for solid $MgCl_2$, of − 201 kJ mol^{-1} for gaseous MeOH and of − 235.1 kJ mol^{-1} for gaseous EtOH was used, respectively [82]

experimentally measured standard enthalpies of reaction. The gravimetric energy density is a thermochemical material characteristic. As a key performance metric, it is used to evaluate and compare the energy storage performance of thermal energy storage systems. The gravimetric energy density of the investigated salt–alcohol systems was similar, irrespective of the reaction pair combination and ranged from 354 to 943 kJ kg^{-1}, respectively. From the energetic point of view, salt–alcohol solvate systems for heat storage are not as good as salt–water solvate systems, as the measured standard enthalpies of reaction and associated gravimetric energy densities are roughly half the respective values of the latter ones [76].

Raman spectroscopic characterization of selected samples

In a starting series of experiments, we increased the laser energy systematically from 200 mW to 500 mW and we found that spectra of sample 6 were not influenced by the change of the excitation energy. This observation let us to conclude that the alcohol solvate sample was stable enough

to be characterized by Raman spectroscopy. Raman spectra of several $CaCl_2$–alcohol solvates recorded at room temperature can be seen in Fig. 8. Comparing the spectrum of pure $CaCl_2$, (line d in Fig. 8a) to those of the different alcohol solvates (lines a, b, e, f in Fig. 8), it could be suggested that the very low wavenumber region was characteristic for $CaCl_2$ and bands from $\sim$ 450 to $\sim$ 3100 cm^{-1} belonged to the alcohols. Although Raman spectroscopy is not actually sensitive to H_2O, a very weak band at about 3400 cm^{-1} indicated that $CaCl_2$ contained a certain amount of coordinated H_2O (line e in Fig. 8b). As a comparison, the Raman spectrum of moisture exposed $CaCl_2$ is also shown (line h in Fig. 8b).

The MeOH in sample 1 (line a in Fig. 8a) was mainly in built-in form as ν_{as} of CH_3 at 2952 cm^{-1} and ν_s of CH_3 at 2844 cm^{-1} and was shifted with $\sim$ 10 cm^{-1} comparing to those of the MeOH (2942 cm^{-1} and 2833 cm^{-1}, line c in Fig. 8a). Bands at 3013 cm^{-1} and 2982 cm^{-1} in sample 1 indicated the presence of coordinated OCH_3 (line a in Fig. 8a), while the band at $\sim$ 3400 cm^{-1} indicated the presence of certain built-in H_2O (cf. line a and line d in Fig. 9a) that was somewhat more intensive than in the starting salt. As the Raman technique gives average information about the material, we could not decide, whether the sample consisted of the mixture of non-coordinated, OH-coordinated, and MeOH-coordinated units of the $CaCl_2$ or units, which had MeOH and H_2O in the same coordination sphere.

Contrary to sample 1, sample 4 contained a large amount of free MeOH besides the coordinated MeOH witnessed by the doublet of ν_s CH_3 band at 2844 cm^{-1} and 2836 cm^{-1}; the latter belongs to non-coordinated MeOH. In addition, a double or triple band in the region $\sim$ 3300 cm^{-1} indicated that –OH and non-coordinated MeOH existed in this sample (cf. lines b and c in Fig. 8a). The appearance of a significant amount of non-coordinated MeOH in sample 4 (prepared at an alcohol/salt ratio of 6:1) confirmed that the maximum number of the coordinated MeOH could be 4, as it was already indicated previously (Sect. 3.1). It is worth noting that the Raman spectrum of sample 3 was very similar to that of sample 4,

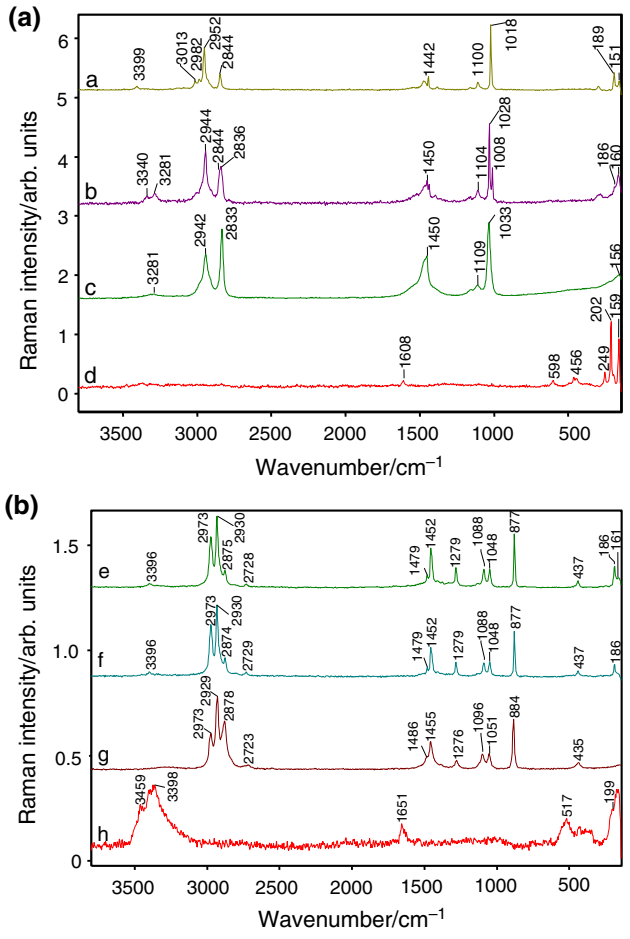

Fig. 8 Raman spectra of alcohol solvates of $CaCl_2$. **a** MeOH solvates; **b** EtOH solvates; a: sample 1; b: sample 4; c: MeOH; d: $CaCl_2$; e: sample 6; f: sample 9; g: EtOH; h: moisture exposed $CaCl_2$

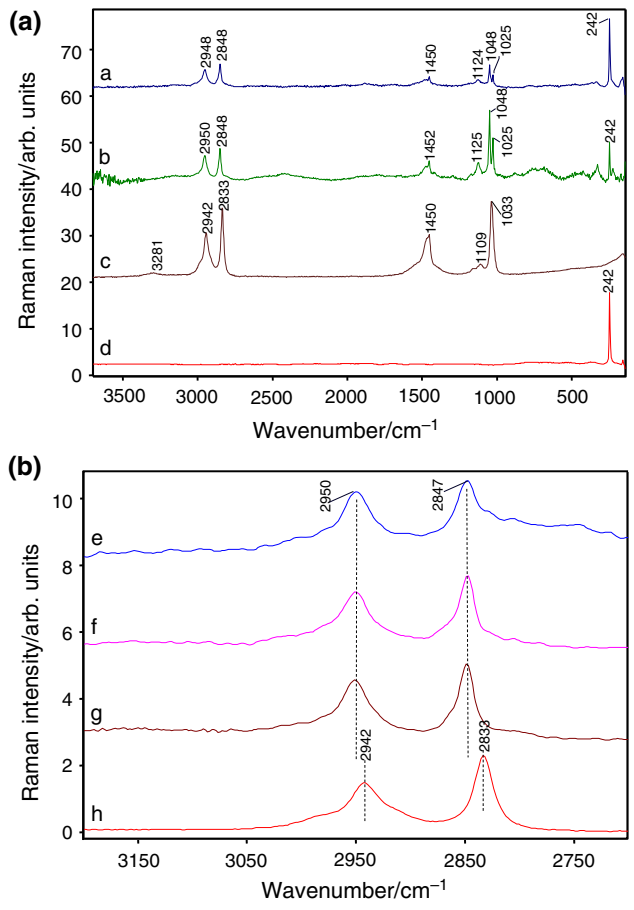

Fig. 9 Raman spectra of MeOH solvates of $MgCl_2$. **a** overview spectra. **b** enlargement of CH_3 region; a: sample 12; b: sample 13; c: MeOH; d: $MgCl_2$; e: sample 10; f: sample 12; g: sample 13; h: MeOH

apart from the band of the non-coordinated MeOH, which was somewhat weaker in sample 3 than in sample 4.

Regarding the alcohol solvates obtained from $CaCl_2$ and EtOH, no real difference between the Raman spectra of the samples prepared at different alcohol/salt ratios could be found (cf. line e and f in Fig. 8b) in accordance with the findings described in Sect. 3.1. Certain relative intensity changes in 2973 cm^{-1}/ ~ 2878 cm^{-1} of $\nu_{as}CH_3/\nu_sCH_3$ in the region of EtOH (cf. lines e, f and g in Fig. 8b) indicated the presence of the EtOH incorporated into the crystal lattice. The shift of the νC-O bands at 1096 cm^{-1} and 1051 cm^{-1} to 1088 cm^{-1} and 1048 cm^{-1}, respectively, could support this idea. However, the appearance of a weak band at 3396 cm^{-1} confirmed again the presence of coordinated H_2O.

Raman spectra of several $MgCl_2$–MeOH solvates are depicted in Fig. 9. Samples in these series were very similar to each other. The splitting of the νC–O band at 1033 cm^{-1} indicated MeOH incorporation into the crystal structure. The intensity ratios of MeOH bands/Mg–Cl bands increased with the amount of introduced MeOH. The ν_{as} of CH_3 appeared at 2950 cm^{-1} and ν_s of CH_3 appeared at 2848 cm^{-1} in the $MgCl_2$–MeOH solvates. These values were shifted compared to that of free MeOH (cf. lines a, b, c and d in Fig. 9b), which indicated that MeOH definitely existed in built-in form in the samples 10, 12, and 13.

Regarding the $MgCl_2$–EtOH systems (Fig. 10), the spectra resembled the spectrum of EtOH showing only negligible band shifts; it was difficult to decide, whether the EtOH existed in a real built-in form or not (cf. line a and c in Fig. 10a). Surprisingly, a new C-H stretching band at high wavenumber appeared (better visualized for sample 18, and only as a shoulder for sample 15) that might be assigned to νC-H of halogen substituted methyl group. As a comparison, the library IR spectrum of ethyl chloride is also shown (Fig. 10b). It seems plausible that ethyl chloride was formed in $MgCl_2$–EtOH systems. Simultaneously, the Ca–Cl vibrational band at 241 cm^{-1} almost completely disappeared (cf. line b in Fig. 10a).

As a conclusion, $MgCl_2$–EtOH solvates underwent certain decomposition resulting in ethyl chloride formation. Pure salt–alcohol solvates could not be obtained, because of the presence of a certain amount of salt hydrates.

TG-MS behavior of selected samples

As preliminary investigations, the starting materials, i.e., the $CaCl_2$ and $MgCl_2$, were analyzed, and it was found that both of them contained roughly around 2% H_2O of crystallization (more precisely, $CaCl_2$ contained 2.28% H_2O, while the H_2O content of $MgCl_2$ was 2.36%).

Four samples were chosen for the TG-MS measurements, namely 3 (containing $CaCl_2$ and MeOH), 7 (which contain $CaCl_2$ and EtOH), 12 (containing $MgCl_2$ and MeOH), and finally 18 (composed of $MgCl_2$ and EtOH). In Fig. 11, the mass loss and some selected ion currents are plotted against the temperature obtained from sample 3,

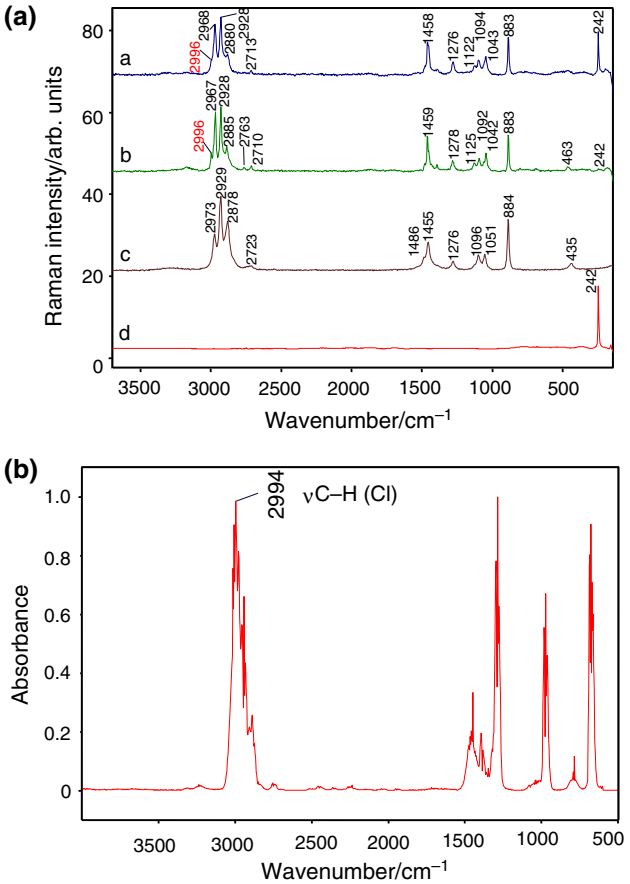

Fig. 10 Raman spectra of $MgCl_2$–EtOH solvates. **a** EtOH solvates; **b** reference FT-IR spectrum of ethyl chloride from Aldrich Vapor FT-IR Spectral Library; a: sample 15; b: sample 18; c: EtOH; d: $MgCl_2$

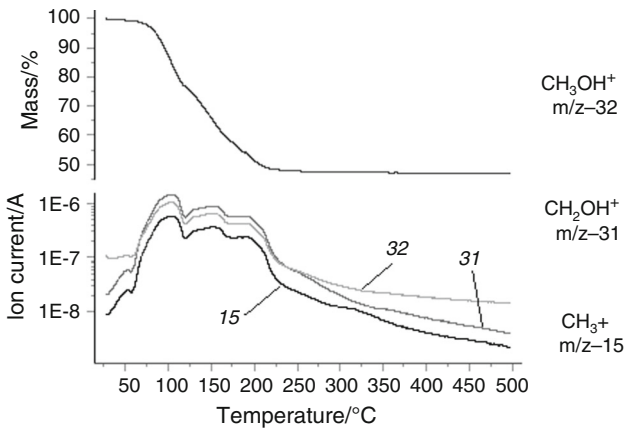

Fig. 11 TG-MS trace of the sample 3 (mass loss on the upper part, while ion currents on the lower part of the graph), on the right side the formulae of the corresponding fragments/ions

while on the right side of the figure the chemical species corresponding to the chosen *m/z* values are also shown. On the TG curve, between 55 and 300.5 °C, three mass loss steps can be seen. The first mass loss step is between 55 and 123.5 °C, with a mass loss of 23.3%, the second step is between 123.5 and 178 °C, with 19.2% mass lost, and the last step between 178 and 300.5 °C resulting in 9.5% mass loss; the total mass loss during the measurement was 52.9%. Comparing the shape of the three ion currents, three overlapping peaks can be observed on each curve, which correspond to the appropriate mass loss step. The *m/z* 32 is the molecular ion of MeOH, the *m/z* 31 is the base peak of MeOH (and also a characteristic marker of aliphatic alcohols), while the *m/z* 15 corresponds to the methyl ion (CH_3). From the TG-MS measurement, it can be concluded that the evolution of MeOH starts at very low temperatures (around 30 °C). Some H_2O was also detected during the measurement (the ion current of H_2O is not shown), but its concentration variation was within one order of magnitude compared to the concentration variation of MeOH, which was 2 orders of magnitude (*m/z* 31), thus confirming that the major volatile component formed during the measurement was MeOH. Moreover, no chlorinated compounds (e.g., methyl chloride) were detected. It can be seen that above 300 °C all three ion current curves are still decreasing, which implies that some MeOH is still lost, but this causes a very small mass loss, not detected by TG.

Considering the TG-MS trace of the sample 7 (Fig. 12), only two mass loss steps can be distinguished. The first mass loss step is between 55 and 95 °C, with a mass loss of 1.9%, while the second step is between 95 and 241 °C, with a mass loss of 48%; the total mass loss during the measurement was 50.3%. It can be seen that the formation of EtOH vapors (*m/z* 46 is the molecular ion of EtOH, *m/z* 45 is a deprotonated EtOH, while *m/z* 31 is the base peak of EtOH) begins at very low temperatures, as already observed in the case of sample 3.

A very small amount of H_2O can be detected between 152 and 235 °C, which means that the H_2O is much more strongly bound to the $CaCl_2$ than the EtOH. No alkyl chloride was detected proving the thermal stability of the $CaCl_2$–alcohol solvate. Comparing the results of sample 3 and 7, it can be concluded that EtOH (sample 7) is lost in a narrower temperature range than MeOH (sample 3). Moreover, the temperature value, where the alcohol is practically lost decreases from 300.5 °C (sample 3) to 240 °C (sample 7). This means that during cyclic measurements, EtOH can be liberated with less energy than MeOH.

Replacing $CaCl_2$ with $MgCl_2$, significant differences appear in the TG-MS trace of sample 12 and 18. On the mass loss curve of the sample 12 (Fig. 13), three mass loss steps can be identified. The first larger step is between 55 and 198 °C, with a mass loss of 40%, the second, smaller mass loss is between 198 and 306 °C (10% mass lost), and the last, very small step is from 306 °C up to the end of the measurement (up to 500 °C, 1.2% mass loss). Evaluating the ion current curves of four masses (*m/z* 32 molecular ion of MeOH, *m/z* 31 base peak of MeOH, while *m/z* 52 is the molecular ion of methyl chloride, with the ^{37}Cl isotope, and *m/z* 50 is the molecular ion of methyl chloride, with the ^{35}Cl isotope), it can be seen that MeOH is liberated below 180 °C. Above this temperature, besides MeOH, which is still the major component of the volatiles and some traces of H_2O, the formation of methyl chloride begins. This confirms that at higher temperatures, $MgCl_2$ hydrolyzes and converts the MeOH into methyl chloride. Around the upper end of the temperature scale, a small amount of methyl chloride is still released between 410 and 490 °C (0.7% mass is lost).

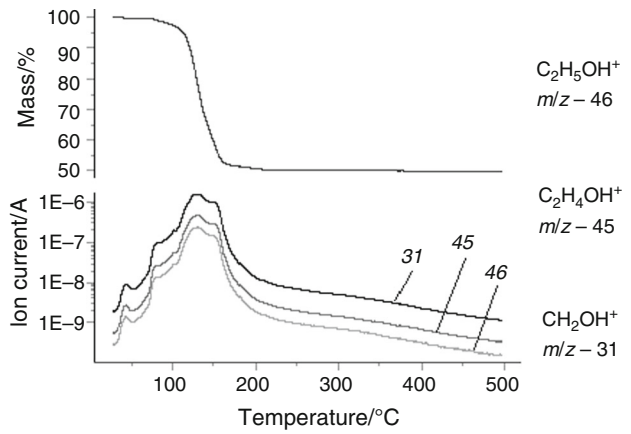

Fig. 12 TG-MS trace of the sample 7, on the right side the formulae of the corresponding fragments/ions

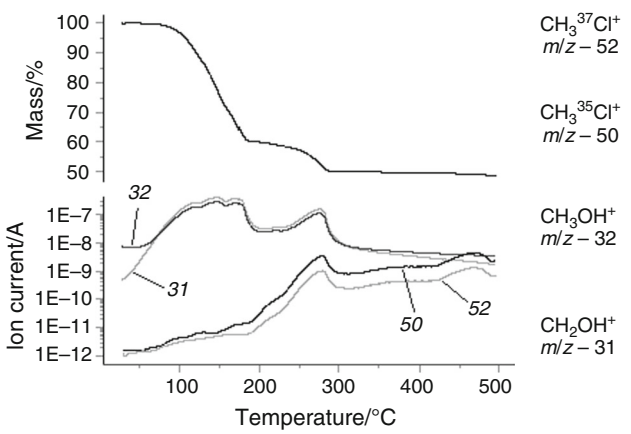

Fig. 13 TG-MS trace of the sample 12, on the right side the formulae of the corresponding fragments/ions

Replacing the MeOH in the magnesium salt with EtOH (sample 18, Fig. 14), again a complicated, multi-step decomposition pattern is obtained. On the mass loss curve of sample 18, four decomposition steps can be identified (first step between 50 and 100 °C, mass loss 4.2%; second, larger step between 100 and 170 °C, mass loss 46.3%, third step between 170 and 212 °C, mass loss 13.3% and fourth step between 212 and 288 °C, mass loss 10.3%). It can be seen that below 140 °C, the mass loss is caused mainly by the evaporation of EtOH (*m*/*z* 46 is the molecular ion of the EtOH, *m*/*z* 45 is a deprotonated EtOH, while *m*/*z* 31 is the base peak of EtOH) and some traces of H_2O (ion curves not shown). Above 140 °C, the formation of ethyl chlorides (*m*/*z* 66 is the molecular ion of ethyl chloride, with the ^{37}Cl isotope, while *m*/*z* 64 is the molecular ion of ethyl chloride, with the ^{35}Cl isotope) can be detected. Ethyl chloride is formed over a broad temperature range (between 140 and 370 °C), additionally the concentration of ethanol decreases above 290 °C, while the ethyl chloride is still formed. The formation of ethyl chloride confirms the fact that $MgCl_2$ hydrolyzes and converts the EtOH into the corresponding alkyl chloride. Comparing the TG-MS results of sample 12 and 18, it can be seen that the alkyl chloride formation starts at lower temperatures in the case of sample 18 (140 °C). The end temperature value of the mass loss end is shifted toward lower temperatures (mass loss end temperature of sample 12 is 306 °C, while the corresponding value is 288 °C in the case of sample 18).

Temperature programmed XRD characterization of selected samples

Figure 15 shows the XRD patterns of four selected salt–alcohol solvate samples recorded by use of stepwise heating. The temperature steps were also chosen according to the TG curve obtained from the TG-MS measurement.

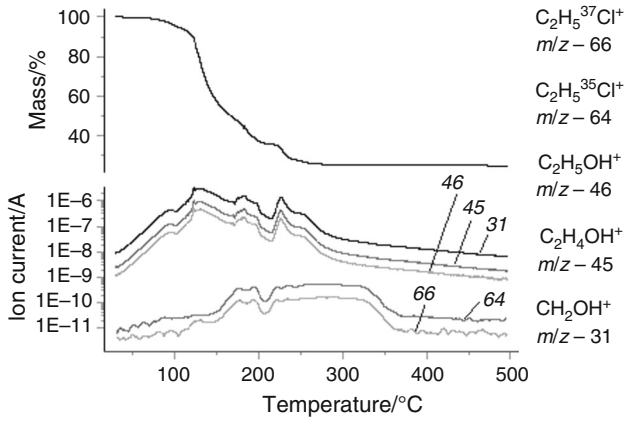

Fig. 14 TG-MS trace of the sample 18, on the right side the formulae of the corresponding fragments/ions

Sample 3 in its starting form (Fig. 15) consisted of MeOH-coordinated phases. The XRD diffraction pattern was somewhat more complicated at 55 °C than at 25 °C, which indicated the formation of a more complex system by the mild heating. These samples consisted of certain $CaCl_2$xMeOH (H_2O) phases. The most likely composition was the average $CaCl_2$/MeOH/H_2O = 1:1:3 ratio in the coordination sphere, which could be estimated from TG. Either a mixture of 1:4 and 1:2 coordinated samples of $CaCl_2$–H_2O and $CaCl_2$–MeOH or samples with mixed coordination spheres could be imagined. At 120 °C, 177 °C, and 301 °C samples were $CaCl_2$-like materials having amorphous part. At 500 °C, only the $CaCl_2$ phase existed. The sample after re-cooling was $CaCl_2$ with some Ca-hydroxide-carbonate. The XRD patterns at 120 °C, 177 °C, and 301 °C were very similar in spite of the large amount of MeOH that went away in the above temperature steps, which implies that a significant amount of MeOH was not really bound in the coordination sphere of the salt.

The diffraction pattern of sample 7 (Fig. 15b) did not change significantly during the heating up to 53 °C in accordance with the TG-MS results, which shows that no significant amount of EtOH or H_2O was removed during the first some minutes. The starting solvate formed at 1:3 molar ratio could be imagined as a mixture of crystals with coordination sphere 1:2 and 1:4 or crystals with coordination sphere 1:2 and alcohol inclusions. The situation was complicated with the presence of H_2O. Consequently, besides the pure $CaCl_2{\cdot}z$EtOH and pure $CaCl_2{\cdot}z H_2O$ crystals, $CaCl_2{\cdot}(x–y)$EtOH$\cdot y H_2O$ structures could exist. Based on the XRD results it was impossible to give a more detailed description. Pure $CaCl_2$ phase could also be found in the region of 55–500 °C. Probably easily decomposable alcoholic, a relatively stable alcoholic and hydrous phases existed parallel in this sample. The final state was alcohol- and H_2O-free $CaCl_2$.

The composition of the initial sample 12 was rather complicated (Fig. 15c). A volatile part was removed at 56 °C that resulted in a slight change in the diffraction pattern. One might think that physisorbed solvent was removed during the heating from 25 up to 56 °C and the solid consisted of mainly several H_2O-coordinated $MgCl_2$ and MeOH-coordinated $MgCl_2$ forms. Regarding the starting solvate, the TG-MS indicated parallel removing of MeOH and a significant amount of H_2O. The TG-MS gave a $MgCl_2$/MeOH ratio of 3.12 only instead of 4. Since the molar mass of H_2O is smaller than that of MeOH, the difference might come from the presence of structures with coordination number 4, but both ligands were in the coordination sphere in different variation. Consequently, the starting solvate itself had to be a mixture. The slight changes in the XRD pattern of sample 12 at 56 °C compared to that at 25 °C resulted from the small variation of

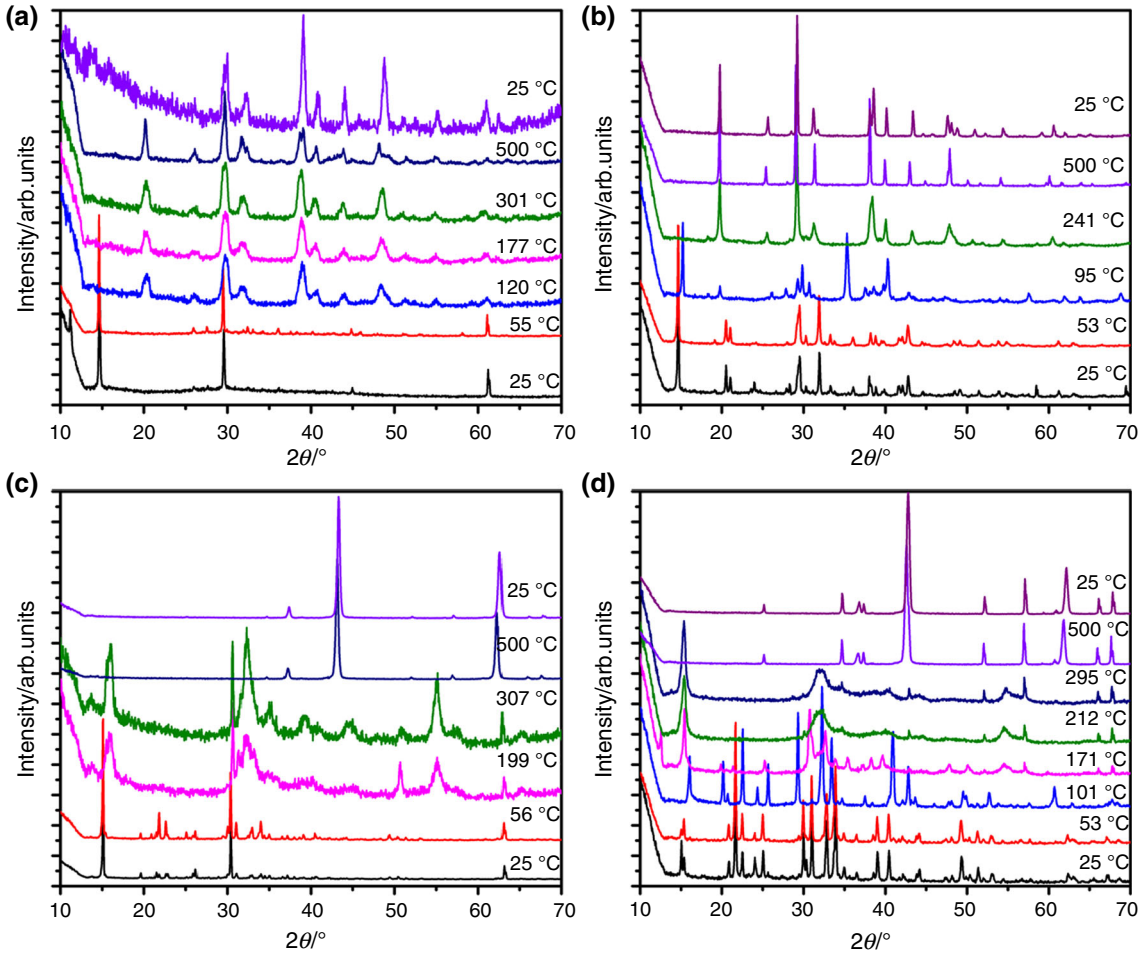

Fig. 15 XRD patterns of selected alcohol solvates at different temperatures (temperature steps adjusted according to TG curve obtained from the TG-MS measurement; heating rate 5 °C min^{-1}; atmosphere: dry N_2). **a** MeOH–$CaCl_2$ (sample 3); **b** EtOH–$CaCl_2$ (sample 7); **c** MeOH–$MgCl_2$ (sample 12); **d** EtOH/$MgCl_2$ (sample 18)

the individual components. At 200 °C, the broadenings in the XRD patterns indicated the formation of amorphous phases. A less crystalline form observed was supposed to be a mixture of MeOH- and H_2O-coordinated materials. It is conceivable that MeOH and H_2O bound to the salt more or less equally strongly. Some small peaks at about $2\theta \sim 32°$ and $2\theta \sim 50°$ decreased upon increasing the temperature, but we can only say that probably the decomposition of 1:2 complexes appeared. At 307 °C either H_2O or MeOH could not be present according to TG-MS. The XRD pattern shows the presence of a certain amount of $MgCl_2$ and/or MgOCl besides amorphous phase(s). At 500 °C, the final material was more crystallized; the final state was MgO (with certain hydrate) and probable Mg-hydroxy-hydrate. The presence of certain MgOOH·HCl could be supposed, too. From these results, it is obvious that the $MgCl_2$ decomposed upon increasing the temperature from 307 to 500 °C. When the sample was cooled to 25 °C, the XRD pattern (and of course the structure) formed at 500 °C was maintained.

The XRD patterns of sample 18 (Fig. 15d) at low temperatures (25 °C, 53 °C) were very similar to those of $MgCl_2{\cdot}zH_2O$. However, TG-MS had shown the removal of mainly EtOH (fragments of EtOH). This observation excluded that the starting material was merely $MgCl_2.zH_2O$. We had to assume that $MgCl_2.zH_2O$ is isostructural with $MgCl_2{\cdot}z$EtOH. Only a little shift of the peaks appeared in comparison with $MgCl_2.zH_2O$, which means that the point group was the same in both cases. Because the shift was small, the cell parameters were not altering significantly. This was very surprising considering the difference in the steric properties of H_2O and EtOH. The very small change in the XRD pattern at 53 °C compared to the XRD pattern at 25 °C could be explained by the removal of a small amount of non-chemisorbed alcohol (physisorbed EtOH or inclusion of EtOH). In the

temperature region of 101–306 °C, the sample gradually lost the EtOH. According to TG-MS results, only EtOH was removed up to 171 °C; EtOH and a small amount of H_2O went away between 171 and 306 °C. Nevertheless, ethyl chloride was also detected by TG-MS indicating a decomposition process. Increasing the temperature from 101 °C up to 212 °C resulted in a change in the XRD patterns with gradual formation of amorphous phases. MgOHCl, $MgCl_2$ (aq) probably existed at higher temperatures. The XRD pattern obtained at 500 °C indicated a cubic crystalline material. The pattern of MgO could be fitted well, but the coexistence of other cubic components could also be suggested. The "temperature programmed" XRD behavior of sample 18 was very similar to that of sample 12.

Results of XRD measurements led us to the following conclusions. Mixtures of different phases containing alcohol and H_2O existed in all of our salt–alcohol solvate samples. $CaCl_2$ was retrievable from its alcohol solvate by bake out of the alcohol solvate, but irreversible processes appeared in case of $MgCl_2$–alcohol solvates. Upon increasing the temperature up to 500 °C, MgO was obtained with elimination of hydrogen chloride similarly to the $MgCl_2{\cdot}6H_2O{\cdot}1,4\text{-}C_4H_8O_2$ [77] and $MgCl_2{\cdot}6H_2O$ system. Although the transformation of the $MgCl_2$ hydrates has long been known [78], clarifying of its mechanism is still in the focus of interest [79].

Possible problems of the applications of salt–alcohol solvates in heat storage systems, based on the results of various techniques used

Our results revealed that the $MgCl_2$–EtOH solvates were instable compound; decomposition of these samples during storage, handling, and analysis was assumed. Raman spectroscopic measurements proved the appearance of ethyl chloride from $MgCl_2$–EtOH without heating. Upon heating, both MeOH and EtOH solvates of $MgCl_2$ were involved in alkyl chloride release, as proven by TG-MS measurements. The alkyl chloride ion current increased slightly from the beginning of the heating and intensified above 140 °C. Although the heating rate can influence on the mechanism of the decomposition, TG-MS measurements by use of high heating rate indicated the formation of alkyl chloride as well as Raman spectroscopy without any heating. On the other hand, XRD measurements showed transformation of $MgCl_2$ in all $MgCl_2$–alcohol solvate samples, which released alkyl chloride.

These observations were in accordance with the literature. Micro-calorimetric analysis has been conducted by Iyimen-Schwarz [51], who has made pioneering scientific contributions to the usability of salt–alcohol solvates based on $CaCl_2/MgCl_2$ and MeOH/EtOH for thermal energy storage. Iyimen-Schwarz [51] calculated the energy density from the forward and reverse reaction enthalpy determined in dynamic DSC measurements under vacuum at controlled temperatures and alcohol vapor pressures. Based on observations on both the shape of the $MgCl_2$–MeOH solvate's measurement curve and the change of the physical appearance, Iyimen-Schwarz suspected the decomposition of the $MgCl_2$–MeOH solvate and the release of CH_3Cl with successive cycling, analogous to the reaction of $MgCl_2$ with H_2O, affecting the reproducibility of the measurements. According to his work, EtOH can be desorbed easily from the $MgCl_2$–ethanolate system. Iyimen-Schwarz further assumed that in this system the $MgCl_2$ is likely to decompose into C_2H_5Cl and HCl, due to unreproducible results of the measured dissociation enthalpy. Results of our TG-MS and Raman spectroscopic measurements fully support the conclusions of Iyimen-Schwarz and explain the poor cyclic stability of $MgCl_2$–EtOH solvates [51].

For alkyl chloride formation in our system different pathways could be assumed. It has been reported that gas phase reaction of EtOH and HCl with formation of H_2O over $ZnCl_2/Al_2O_3$ as a catalyst, is a suitable method for ethyl chloride preparation [80]. According to a possible explanation, the starting material ($MgCl_2$) contains $MgCl_2{\cdot}zH_2O$ in the presence of traces of H_2O. Heating the $MgCl_2$ hydrates results in $MgOH_xCl_x$ with probable formation of hydrochloric acid (HCl). At the same time, reaction of alcohols and HCl can lead to the formation of methyl chloride (CH_3Cl), or ethyl chloride (C_2H_5Cl) via $MgCl_2$ acting as a catalyst. Deliberation of H_2O carries on the decomposition of $MgCl_2$. A direct interaction between the ligands (i.e., Cl^- and alcohol) in the coordination sphere of the Mg^{2+} can also be assumed. This idea does not need the H_2O to assist in the alkyl chloride formation, but it can lead to the gradual hydrolysis of $MgCl_2$. Although we do not have direct evidence for the first or second pathway, we believe that the direct way is more likely, since ethyl chloride formation appeared even at room temperature, while HCl release from $MgCl_2{\cdot}2H_2O$ was reported only at 167 °C [79]. It is worth to note that the final temperature in the cyclic stability test of $MgCl_2{\cdot}z$EtOH was 180 °C [29].

The results presented in Sect. 3.3–3.5 demonstrate that pure salt–alcohol solvates could not be prepared under technically applicable conditions; the samples contained at least traces of H_2O. H_2O could be introduced by both the preparation procedure and by the starting materials, despite the use of commercial absolutized solvents and N_2

atmosphere for the preparation. The starting salts also contained 1–2% of H_2O, which resulted in the presence of salt hydrates besides the mixture of salt–alcohol solvates. The possibility of the formation of salt hydrates implies the possibility of HCl formation during the thermal treatment above 167 °C [81]. In practical applications, an inert atmosphere cannot be maintained during the whole process, so that traces of H_2O cannot be avoided. Additionally, the use of high purity grade H_2O-free substances might be too expensive at technical scale. The appearance of side reactions and the release of HCl with cycling can contribute to corrosion of the reactor components. The decomposition of $MgCl_2$–alcohol solvates results further in a degradation of the overall performance of the thermal energy storage system. In conclusion, the reaction system $MgCl_2$·R-OH is not suitable for practical implementation, due to its instability and irreversibility. From the energetic point of view, this compound is also not favorable as the measured enthalpies of reaction and associated energy densities are lower than that of $CaCl_2$–alcohol solvates and salt-H_2O systems [76].

Conclusions

Reversible chemical reactions are highly efficient in terms of storage volume, storage period, and sensible heat losses to the environment compared to other energy storage technologies. Different $CaCl_2$- and $MgCl_2$–alcohol solvates (EtOH, MeOH) were synthesized and their suitability for heat storage was examined by employing combined thermogravimetric analysis and differential scanning calorimetry (TGA/DSC), spectrometric and spectroscopic analysis (TG-MS, Raman) methods as well as by using X-ray diffraction (XRD). Due to their chemical nature, the $CaCl_2$–EtOH systems exhibited lower energy densities than $CaCl_2$-H_2O systems. Decomposition of $MgCl_2$–EtOH solvates accompanied by ethyl chloride formation started already during storage. Upon heating, both MeOH and EtOH solvates of $MgCl_2$ were affected by alkyl chloride release, as proven by TG-MS measurements. Our results fully support the assumptions of Iyimen-Schwarz [51] and explain the poor cycle stability of $MgCl_2$–EtOH solvates reported previously. We also demonstrated that pure salt–alcohol solvates cannot be prepared under technically applicable conditions. Formation of salt hydrates implies the possibility of HCl formation during the thermal treatment. Appearance of side reactions and possible release of HCl with cycling may be conducive to corrosion. Conclusively, $MgCl_2$–alcohol solvate systems are not recommended for heat storage, whereas $CaCl_2$–alcohol systems are suitable demonstrating stable cycle performance. The information on the decomposition pattern and associated changes in the structural integrity of the salt alcoholates obtained in this study are essential for selecting and designing efficient thermochemical energy stores. The fundamental data on the heat content of the parent salt provide the basis for the development of new two-component thermochemical materials with advanced properties.

Acknowledgements Open access funding provided by MTA Research Centre for Natural Sciences (MTA TTK). Project no. TÉT_12_DE-1-2013-0003 has been implemented with the support provided by the National Research, Development and Innovation Fund of Hungary, financed under the TÉT_12_DE funding scheme. This study received funding from the German Federal Ministry of Education and Research (BMBF) within the framework of a bilateral research collaborative project between the Leuphana University of Lüneburg and the Hungarian Academy of Sciences under grant agreement number 01DS14029. The authors thank Christina Apel for the preparation of salt–alcohol solvate samples.

Appendix 1: Calculations

The alcohol/salt molar ratios (levels of alcoholation) were derived from experimental data obtained by TGA. The percentage mass loss X is defined as the mass of alcohol $m_{\text{R-OH}}$ desorbed per unit mass of salt alcoholate $m_{\text{MX ZR-OH}}$:

$$X = \frac{m_{\text{R-OH}}}{m_{\text{MXzR-OH}}} 100\% \tag{3}$$

The level of alcoholation z is defined as the ratio of the number of alcohol molecules evolved during the endothermic dissociation reaction $n_{\text{R-OH}}$ to the amount of anhydrous salt n_{MX} and was calculated from the following equation:

$$z = \frac{n_{\text{R-OH}}}{n_{\text{MX}}} = \frac{m_{\text{R-OH}} M_{\text{MX}}}{m_{\text{MX}} M_{\text{R-OH}}} \tag{4}$$

wherein m_{MX} and $m_{\text{R-OH}}$ are the masses of the anhydrous salt and the alcohol desorbed, respectively.

The principle of thermochemical heat storage using reversible gas–solid reactions is based on the conversion of thermal energy into chemical energy required to break the chemical bonds of the reactants. At constant pressure, the amount of heat energy that must be supplied to induce the decomposition reaction equals the endothermic heat of reaction, also designated enthalpy of reaction. An infinitesimal change in the temperature results in a change

of the enthalpy by $\Delta C_p dT$. The enthalpy of reaction $\Delta_r H$ under non-standard condition, in case of a reaction temperature T_1 different from the standard state temperature T_0 can be estimated from the standard reaction enthalpies and heat capacities of the reactants using Kirchhoff's law. The heat energy ΔQ is then expressed by:

$$\Delta Q = \Delta_r H(T_1, p_0) = \Delta_r H^0(T_0, p_0) + \int_{T_0}^{T_1} \Delta C_p dT + \Delta_{Tr} H \tag{5}$$

where $\Delta rH^0(T_0)$ is the standard enthalpy of reaction at standard state conditions T_0 = 298.15 K and p_0 = 1 bar, C_p is the constant-pressure heat capacity and $\Delta_{Tr} H$ is the enthalpy of transformation.

The enthalpy of reaction was obtained from DSC measurement by peak area integration. The energy that is liberated or absorbed as heat during a chemical reaction as a result of a temperature difference ΔT can be quantitatively determined by heat flux DSC. This technique measures the thermally induced heat flux transferred between the sample and an inert reference that are connected by a low-resistance heat flow path. Thermocouples below the symmetrically positioned sample crucible and empty reference crucible detect and compare the temperature of the specimen to the temperature of the reference as a function of time under same conditions. The heat flux between sample and reference is proportional to the temperature difference:

$$\phi = E_{(T)} \mathrm{DSC} = E_{(T)} \Delta T \tag{6}$$

wherein $E_{(T)}$ and DSC are the calorimetric sensitivity and the measured DSC signal. Integration of the peak area under the baseline-subtracted DSC signal over time yields $\Delta_r H^0$:

$$\Delta_r H^0 = \int_{t_1}^{t_2} \mathrm{DSC}\, dt = \int_{t_1}^{t_2} \frac{\phi}{E_{(T)}} dt \tag{7}$$

According to Hess Law, the value of the standard reaction enthalpy of the forward and reverse reaction must be equal and the same applies for the standard enthalpy of association and standard enthalpy of dissociation. The standard enthalpy of dissociation is the inverse of the standard enthalpy of formation. In general, the standard enthalpy of reaction is calculated from the difference of the standard enthalpy of formation of the products and the standard enthalpy of formation of the reactants:

$$\Delta_r H^0 = \sum \Delta_f H^0_{\text{products}} - \sum \Delta_f H^0_{\text{reactants}} \tag{8}$$

Solving Eq. (8) for $\Delta_f H^0_{\text{products}}$ gives the standard enthalpy of formation and hence the standard enthalpy of dissociation.

Different mathematical approaches are used to determine the specific energy storage density. Two types of energy densities are known: gravimetric and volumetric energy density. The gravimetric energy density E_m is defined as the capacity of heat energy stored at a defined temperature and pressure per unit mass of storage material and can be calculated from the ratio of the standard reaction enthalpy to the molar mass of the reactant $M_{\text{MX zR-OH}}$:

$$E_m = \frac{\Delta_r H^0}{M_{\text{MX zR-OH}}} \tag{9}$$

whereas the volumetric energy density E_V is related to the volume of storage material and is described as:

$$E_V = \frac{\Delta_r H^0}{M_{\text{MX zR-OH}}} \rho \tag{10}$$

The storage material volume is derived from the material's mass and bulk density ρ. The higher the level of alcoholation, the lower is the density. The volumetric energy density is an important key energy storage metric for designing and operating storage systems. It is also preferred for performance comparison studies. Space can be a limiting factor for many practical applications. There are no data available for the mass and bulk densities of the salt–alcohol systems studied and hence only the gravimetric energy density could be calculated.

Appendix 2: Data processing—example of a TGA/DSC curve

Figure 16 displays the DSC measurement curve and corresponding TGA signal normalized to the sample mass for sample 6. To determine the heat content of the sample and the associated enthalpy of reaction, the area under the DSC peak was integrated. Similar curves were recorded for all other samples.

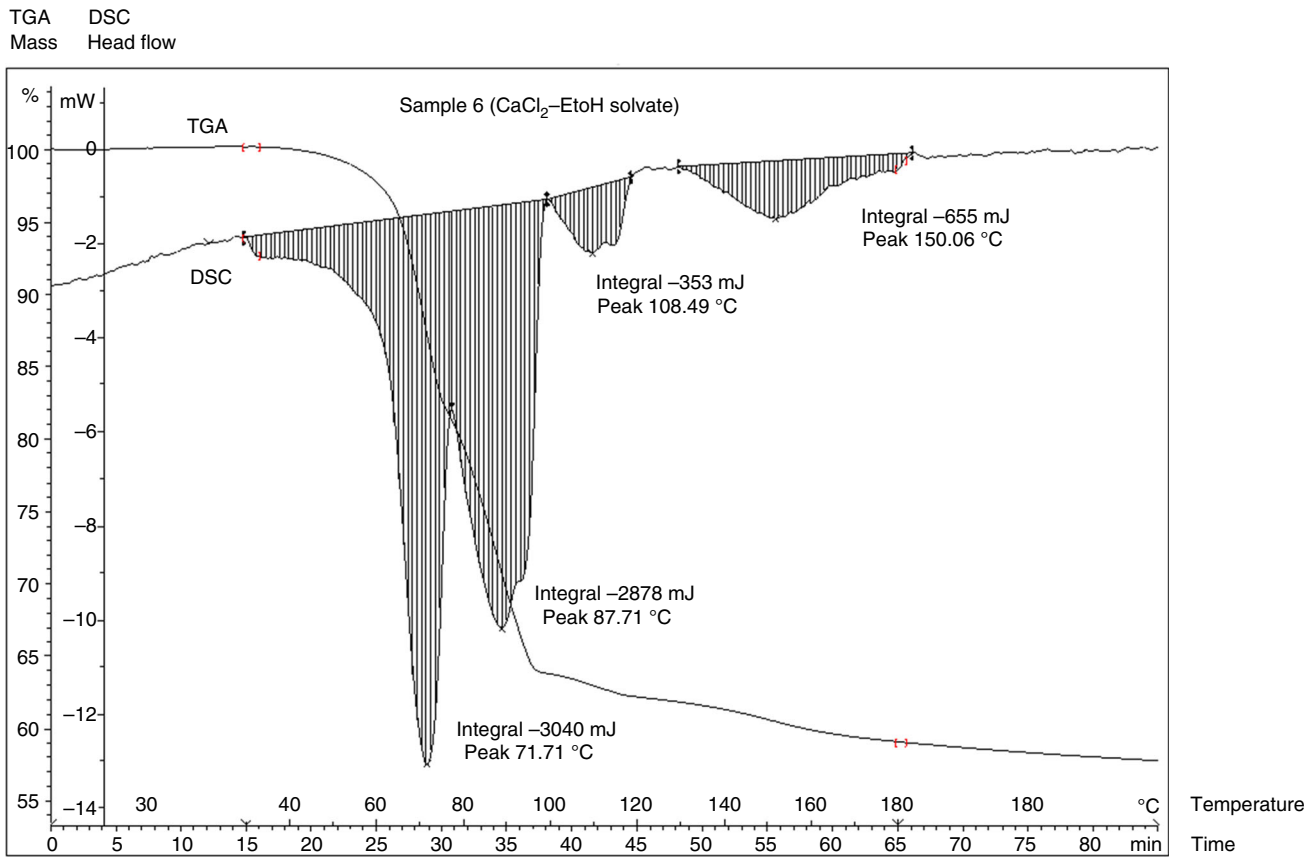

Fig. 16 Example of a recorded TGA and DSC curve. The TGA curve or change in mass (%) and DSC curve or heat flow (mW) are given as a function of time (min) and temperature (°C). The sample was heated from 30 to 180 °C at a heating rate of 3 K min^{-1}. Since the signs of the thermal processes were inverted due to software issues, the signed number of the underlying endothermic reaction is negative

References

1. Dincer I, Rosen MA. Thermal energy storage systems and applications. Chichester: Wiley; 2002.
2. Garg HP, Mullick SC, Bhargava AK. Solar thermal energy storage. Dodrecht: D. Reidel Publishing Company; 1985.
3. Agyenim F, Hewitt N, Eames P, Smyth M. A review of materials, heat transfer and phase change problem formulation for latent heat thermal energy storage systems (LHTESS). Renew Sustain Energy Rev. 2010;14:615–28.
4. Feczkó T, Trif L, Horák D. Latent heat storage by silica-coated polymer beads containing organic phase change materials. Sol Energy. 2016;132:405–14.
5. Kenfack F, Bauer M. Innovative phase change material (PCM) for heat storage for industrial applications. Energy Proc. 2014;46:310–6.
6. Naumann R, Emons HH. Results of thermal analysis for investigation of salt hydrates as latent heat-storage materials. J Therm Anal Calorim. 1989;35:1009–31.
7. Naumann R, Schatz O. Thermoanalytical investigation of some alkaline earth hydroxidehydrates on application as latent heat storage materials. J Therm Anal Calorim. 1992;38:665–71.
8. Sharma A, Tyagi VV, Chen CR, Buddhi D. Review on thermal energy storage with phase change materials and applications. Renew Sustain Energy Rev. 2009;13:318–45.
9. Zhang N, Yuan Y, Cao X, Du Y, Zhang Z, Gui Y. Latent heat thermal energy storage systems with solid–liquid phase change materials: a review. Adv Eng Mater. 2018;20:1700753. https://doi.org/10.1002/adem.201700753.
10. Anghel EM, Georgiev A, Petrescu S, Popov R, Constantinescu M. Thermo-physical characterization of some paraffins used as phase change materials for thermal energy storage. J Therm Anal Calorim. 2014;117:557–66.
11. Kong W, Lei Y, Jiang Y, Lei J. Preparation and thermal performance of polyurethane/PEG as novel form-stable phase change materials for thermal energy storage. J Therm Anal Calorim. 2017;130:1011–9.
12. Guo L, Yu X, Gao D, Guo Y, Ma C, Deng T. Synthesis and thermal energy storage properties of a calcium-based room temperature phase change material for energy storage. J Therm Anal Calorim. 2018. https://doi.org/10.1007/s10973-018-7610-3.
13. He Y, Zhang N, Yuan Y, Cao X, Sun L, Song Y. Improvement of supercooling and thermal conductivity of the sodium acetate trihydrate for thermal energy storage with α-Fe_2O_3 as addictive. J Therm Anal Calorim. 2018;133:859–67.
14. Cui W, Zhang H, Xia Y, Zou Y, Xiang C, Chu H, et al. Preparation and thermophysical properties of a novel form-stable $CaCl_2{\cdot}6H_2O$/sepiolite composite phase change material for latent heat storage. J Therm Anal Calorim. 2018;131:57–63.
15. Genc M, Karagoz Genc Z. Microencapsulated myristic acid–fly ash with TiO_2 shell as a novel phase change material for building application. J Therm Anal Calorim. 2018;131:2373–80.

16. Bevers ERT, Oonk HAJ, Haije WG, van Ekeren PJ. Investigation of thermodynamic properties of magnesium chloride amines by HPDSC and TG. J Therm Anal Calorim. 2007;90:923–9.
17. Jabbari-Hichri A, Bennici S, Auroux A. Water sorption heats on silica-alumina-based composites for interseasonal heat storage. J Therm Anal Calorim. 2014;118:1111–8.
18. Posern K, Osburg A. Determination of the heat storage performance of thermochemical heat storage materials based on $SrCl_2$ and $MgSO_4$. J Therm Anal Calorim. 2018;131:2769–73.
19. Posern K, Kaps C. Humidity controlled calorimetric investigation of the hydration of $MgSO_4$ hydrates. J Therm Anal Calorim. 2008;92:905–9.
20. Lager D, Hohenauer W, Knoll C, Weinberger P, Werner A. Methodology to determine the apparent specific heat capacity of metal hydroxides for thermochemical energy storage. J Therm Anal Calorim. 2018;133:207–15. https://doi.org/10.1007/s10973-017-6883-2.
21. Bevers ERT, van Ekeren JP, Haije WG, Oonk HAJ. Thermodynamic properties of lithium chloride ammonia complexes for application in a high-lifthigh temperature chemical heat pump. J Therm Anal Calorim. 2006;86:825–32.
22. Ishitobi H, Uruma K, Takeuchi M, Ryu J, Kato Y. Dehydration and hydration behavior of metal-salt-modified materials for chemical heat pumps. Appl Therm Eng. 2013;50:1639–44.
23. Donkers PAJ, Pel L, Adan OCG. Experimental studies for the cyclability of salt hydrates for thermochemical heat storage. J Energy Storage. 2016;5:25–32.
24. Hamdan MA, Rossides SD, Haj Khalil R. Thermal energy storage using thermo-chemical heat pump. Energy Convers Manag. 2013;65:721–4.
25. Korhammer K, Druske MM, Fopah-Lele A, Rammelberg HU, Wegscheider N, Opel O, Osterland T, Ruck W. Sorption and thermal characterization of composite materials based on chlorides for thermal energy storage. Appl Energy. 2016;162:1462–72.
26. Posern K, Kaps Ch. Calorimetric studies of thermochemical heat storage materials based on mixtures of $MgSO_4$ and $MgCl_2$. Thermochim Acta. 2010;502:73–6.
27. Carling RW, Wondolowski AT, Macmillan DC. Enthalpy of formation of $CaCl_2x2CH_3OH$ and $CaCl_2x{\cdot}2C_2H_5OH$ by solution calorimetry. J Chem Thermodyn. 1982;14:125–31.
28. Cho HS, Lee WY. Synthesis of inorganic $MgCl_2$–alcohol adduct via recrystallization method and its application in supported organometallic catalysts for the polymerization of ethylene with 1-hexene. J Mol Catal A-Chem. 2003;191:155–65.
29. Korhammer K, Apel C, Osterland T, Ruck WKL. Reaction of calcium chloride and magnesium chloride and their mixed salts with ethanol for thermal energy storage. Energy Proc. 2016;91:161–71.
30. Muroyama AP, Schrader AJ, Loutzenhiser PG. Solar electricity via an Air Brayton cycle with an integrated two-step thermochemical cycle for heat storage based on Co_3O_4/CoO redox reactions II: kinetic analyses. Sol Energy. 2015;122:409–18.
31. Olivares R, Edwards W. $LiNO_3$–$NaNO_3$–KNO_3 salt for thermal energy storage: thermal stability evaluation in different atmospheres. Thermochim Acta. 2013;560:34–42.
32. Kousksou T, Jamil ĆA, Gibout ĆS, Zeraouli YĆ. Thermal analysis of phase change emulsion. J Therm Anal Calorim. 2009;96:841–52.
33. Anghel EM, Georgiev A, Petrescu S, Popov R, Constantinescu M. Thermo-physical characterization of some paraffins used as phase change materials for thermal energy storage. J Therm Anal Calorim. 2014;117:557–66.
34. Wong B, Brown L, Buckhingham R, Sweet W, Russ B, Gorensek M. Sulfur dioxide disproportionation for sulfur based thermochemical energy storage. Sol Energy. 2015;118:134–44.
35. van Essen VM, Zondag HA, Gores JC, Bleijendaal LPJ, Bakker M, Schuitema R, van Helden WGJ, He Z, Rindt CCM. Characterization of $MgSO_4$ hydrate for thermochemical seasonal heat storage. J Sol Energy Eng. 2009;131:041014-1–7.
36. van Essen VM, Bleijendaal LPJ, Kikkert BWJ, Zondag HA, Bakker M, Bach PW. Development of a compact heat storage system based on salt hydrates. In: Proceedings of the EUROSUN; 2010.
37. Zondag H, van Essen M, Bleijendaal L, Cot J, Schuitema R, Planje W, Epema T, Oversloot H. Comparison of reactor concepts for thermochemical storage of solar heat. In: Third International Renewable Energy Storage Conference, IRES; 2008:24–5.
38. Aristov YI, Gordeeva LG, Pankratiev YD, Plyasova LM, Bikova IV, Freni A, Restuccia G. Sorption equilibrium of methanol on new composite sorbents "$CaCl_2$/silica gel". Adsorption. 2007;13:121–7.
39. Gillier-Pandraud H, Philoche-Levisalles M. Structure cristalline du compose $CaCl_2$ CH_3OH. C R Acad Sci Ser C. 1971;273:949–51.
40. Hirata Y, Fujioka K. Thermophysical properties and heat transfer characteristics of $CaCl_2$ heat pump reactor associated with structural change of reactive salts. In: V Minsk international seminar ''Heat pipes, heat pumps, refrigerators''; 2003.
41. Lai H, Li C. Application of periodic reversal flow reactors to chemical heat pump systems based on solid/vapor non-catalytic reaction. Chem Eng Sci. 1996;51:2951–7.
42. Offenhartz PO'D, Brown FC, Mar RW, Carling RW. A heat pump and thermal storage system for solar heating and cooling based on the reaction of calcium chloride and methanol vapor. J Sol Energy Eng. 1980;102:59–65.
43. Gmelin L. Handbuch der anorganischen chemie. Weinheim: Verlag Chemie; 1966.
44. Bonnell DGR, Jones WJXLII. The dissociation pressures of alcoholates. Part I. J Chem Soc (Resumed). 1926;129:321–8.
45. Menschutkin BN. Über einige Kristallalkoholate. Zeitschrift für anorganische und allgemeine Chemie. 1907;52:9–24.
46. Brusset H, Gillier-Pandraud H, Philoche-Levisalles M. Crystallographic data on compound $CaCl_2$. C R Acad Sci Ser C. 1970;271:579.
47. Halut-Desportes S, Husson E. Spectres d'absorption infrarouge et calcul de champ de force de complexes de coordination: halogénures de magnésium et de calcium avec le méthanol ou l'éthanol. Spectrochim Acta A Mol Spectr. 1985;41:661–73.
48. Kane R. Beiträge zur Geschichte des Holzgeistes und seiner Verbindungen. Eur J Org Chem. 1836;19:164–83.
49. Halut-Desportes S, Philoche-Levisalles M. Structures comparées des solvates de formule MBr_2. $6CH_3OH$. Acta Crystallogr B-Struct Crystallogr Cryst Chem. 1978;34:432–5.
50. Mar RW, Carling RW. The calcium chloride—ethanol system. Thermochim Acta. 1981;45:213–7.
51. Iyimen-Schwarz, Z. Energiespeicherung durch chemische Reaktionen. Doctoral dissertation; 1984.
52. Heindl JB. Über krystallinische Verbindungen von Chlorcalcium mit Alkoholen. Monatshefte für Chemie und verwandte Teile anderer Wissenschaften. 1881;2:200–11.
53. Parker VB, Wagman DD, Evans WH. NBS Technical Note 270-6. Selected values of thermodynamic properties. Washington: US Government Printing Office; 1971.
54. von Chodnew A. Beiträge zur Kenntniss der Alkoholate und der salpetersauren Magnesia. Eur J Org Chem. 1849;71:241–65.
55. Graham T. XLVII. An account of the formation of alcoates, definite compounds of salts and alcohol analogous to the hydrates. Philos Mag Ser. 1828;2(4):265–72.
56. Multani RK. Action of magnesium chloride on alcohols. Curr Sci. 1964;33:430.

57. Olmer LJ, Quinet MLB. Soc Chim Fr. 1934;1:1579–81.
58. Choi JH, Chung JS, Shin HW, Song IK, Lee WY. The effect of alcohol treatment in the preparation of $MgCl_2$ support by a recrystallization method on the catalytic activity and isotactic index for propylene polymerization. Eur Polym J. 1996;32:405–10.
59. Quinet MLB. Soc Chim Fr. 1936;3:1829.
60. Emons HH, Pollmer K. Studies on systems of salts and mixed solvents. XXXI. On the solubility and solvation behaviour of magnesium chloride in mixed aqueous organic solvents. Zeitschrift für anorganische und allgemeine Chemie. 1985;521:224–30.
61. Gnanakumar ES, Gowda RR, Kunjir S, Ajithkumar TG, Rajamohanan PR, Chakraborty D, Gopinath CS. $MgCl_2{\cdot}6CH_3OH$: a simple molecular adduct and its influence as a porous support for olefin polymerization. ACS Catal. 2013;3:303–11.
62. Kabisch G, Bader I, Emons HH, Pollmer K. A Raman spectroscopic investigation of the structure of magnesium salt solutions in methanol and methanol-water mixtures. J Mol Liq. 1983;26:139–57.
63. Lloyd E, Brown CB, Bonnell DGR, Jones WJ. XC.—Equilibrium between alcohols and salts. Part II. J. Chem. Soc. (Resumed). 1928;658–66. https://doi.org/10.1039/JR9280000658
64. Radnai T, Kalman E, Pollmer K. X-ray diffraction study of $MgCl_2$ in methanol. Z Naturforsch Pt A. 1984;39:464–70.
65. Simon SE. Über die Verbindungen des Chlorlithiums und des Chlormagnesiums mit Alkoholen. Adv Synth Catal. 1879;20:371–7.
66. Turova NY, Turevskaya EP. Alkoxymagnesium halides. J Organomet Chem. 1972;42:9–17.
67. Nasirzadeh K, Zimin D, Neueder R, Kunz W. Vapor-pressure measurements of liquid solutions at different temperatures: apparatus for use over an extended temperature range and some new data. J Chem Eng Data. 2004;49:607–12.
68. Tewell CR, Malizia F, Ager JW, Somorjai GA. An ultraviolet–Raman spectroscopic investigation of magnesium chloride–ethanol solids with a 0.47 to 6 molar ratio of C_2H_5OH to $MgCl_2$. J Phys Chem B. 2002;106:2946–9.
69. Chadwick JC, Severn JR. Single-site catalyst immobilization using magnesium chloride supports. Kinet Catal. 2006;47:186–91.
70. Bart JCJ, Roovers W. Magnesium chloride-ethanol adducts. J Mater Sci. 1995;30:2809–20.
71. Di Noto V, Zannetti R, Vivani M, Marega C, Marigo A, Bresadola S. $MgCl_2$-supported Ziegler–Natta catalysts: a structural investigation by X-ray diffraction and Fourier-transform IR spectroscopy on the chemical activation process through $MgCl_2$-ethanol adducts. Macromol Chem Phys. 1992;193:1653–63.
72. Malizia F, Fait A, Cruciani G. Crystal structures of Ziegler–Natta catalyst supports. Chem Eur J. 2011;17:13892–7.
73. Jiang X, Tian X, Fan Z. Crystal structure of ball-milled mixture of sodium chloride and magnesium chloride–ethanol adduct. Mater Res Bull. 2008;43:343–52.
74. Taveira Magalhaes DN, Do Coutto Filho O, Coutinho FMB. Ziegler-Natta catalyst for ethylene and propylene polymerization supported on adducts of magnesium chloride with methyl and ethyl alcohols. Eur Polym J. 1991;27:827–30.
75. Thushara KS, Gnanakumar ES, Mathew R, Ajithkumar TG, Rajamohanan PR, Bhaduri S, Gopinath CS. $MgCl_2\bullet\ 4((CH_3)_2CHCH_2OH)$: a new molecular adduct for the preparation of $TiCl_x/MgCl_2$ catalyst for olefin polymerization. Dalton Trans. 2012;41:11311–8.
76. N'Tsoukpoe KE, Schmidt T, Rammelberg HU, Watts BA, Ruck WK. A systematic multi-step screening of numerous salt hydrates for low temperature thermochemical energy storage. Appl Energy. 2014;124:1–16.
77. Jin M, Sun Y, Li P, Yu J, Ulrich J. The thermal decomposition study of $MgCl_2{\cdot}6H_2O{\cdot}1,4\text{-}C_4H_8O_2$. Chem Eng Res Des. 2015;104:256–63.
78. Galwey AK, Laverty GM. The thermal decomposition of magnesium chloride dihydrate. Thermochim Acta. 1989;138:115–27.
79. Huang Q, Lu G, Wang J, Yu J. Mechanism and kinetics of thermal decomposition of $MgCl_2x6H_2O$. Metall Mater Trans B. 2010;41:1059–66.
80. Bukhanko N, Samikannu A, Larsson W, Shchukarev A, Leino AR, Kordás K, Warna J, Mikkola JP. Continuous gas-phase synthesis of ethyl chloride from ethyl alcohol and hydrochloric acid over Al_2O_3 based catalysts: the "green" route. ACS Sustain Chem Eng. 2013;1:883–93.
81. Huang Q, Lu G, Wang J, Yu J. Thermal decomposition mechanisms of $MgCl_2{\cdot}6H_2O$ and $MgCl_2{\cdot}H_2O$. J Anal Appl Pyrol. 2011;91:159–64.
82. Wagman DD, Evans WH, Parker VB, Schumm RH, Halow I. The NBS tables of chemical thermodynamic properties. Selected values for inorganic and C1 and C2 organic substances in SI units. National Standard Reference Data System, 1982.